Progress In Electromagnetics Research B, Vol. 96, 39–66, 2022

Design Consideration, Challenges and Measurement Aspects of 5G mm-Wave Antennas: A Review

Ashok Kumar[1, *], Ashok Kumar[2], Ping Jack Soh[3], and Arjun Kumar[1]

Abstract—With the supersonic growth of mobile data demand, the fifth generation (5G) mobile network would exploit the extensive amount of spectrum in the millimeter-wave (mm-Wave) bands to tremendously increase communication capacity. There are conceptual differences between mm-Wave communications and other existing communication systems, in terms of high propagation loss, directivity, and sensitivity to blockage. These characteristics of mm-Wave communications present several challenges to completely exploit the potential of mm-Wave communications, including integrated circuits and system design, interference management, spatial reuse, anti-blockage, and dynamics control. 5G mobile communication systems with sub-6 GHz and millimeter-wave bands are already replacing 4G and 4.5G systems as an evolution towards higher-speed mobile communication and wider bandwidth. From the hardware perspective, the 5G-band causes the miniaturization of RF components including the antennas. In this article, an overview of recent research is presented that discusses design challenges and measurement considerations for various types of compact 5G antennas.

1. INTRODUCTION

Over the last few decades, there is a rapid evolution of modern wireless communications from simple voice systems to advanced multimedia communications in terms of video calling, video chat, and device connectivity with the internet of things (IoT) [1–3]. It is evident that the social activities of human life in daily life and the need for wireless devices increase. Mobile connections and mobile data traffic are increasing exponentially [4]. Hence it has been seen that after every decade, the data consumption became at least doubled with wireless and multimedia uses. The fourth generation (4G) technology was successfully launched in 2009 in Norway and Sweden followed by other countries worldwide. The 4G network operates in the frequency band of 700 MHz, 850 MHz, 950 MHz, 1800 MHz, 1900 MHz, 2100 MHz, 2300 MHz, and 2600 MHz. The international telecommunication union (ITU) recommended a maximum data speed of one gigabits per second (Gbps) for high-speed mobile users like trains, cars, airplanes, and 100 megabits per second (Mbps) for low-speed mobile users as walking on roads [5, 6]. By using an IP packet switching network, 4G technology can connect multiple users per cell, provide better coverage and uninterrupted connectivity, especially for video chats and conferences [7]. Having utilities, there were some limitations of the current mobile network which deployed the research community towards better technology. The major drawbacks of 4G technology are included in terms of limited device connectivity as up to 4000 devices per square kilometer hence not supported by IoT, low latency of around 20 milliseconds, which is not suitable for real-time communication, and small bandwidth. Although various telecom industries and researchers are doing their best to enhance the data rate and radiation characteristics, they failed to fulfill the consumer demands [8, 9].

Received 20 May 2022, Accepted 8 July 2022, Scheduled 27 July 2022

* Corresponding author: Ashok Kumar (ashokmzn@gmail.com).

[1] School of Engineering and Applied Sciences, Bennett University, Greater Noida, Uttar Pradesh, India. [2] Department of Electronics and Communication Engineering, Government Mahila Engineering College, Ajmer, Rajasthan, India. [3] Centre for Wireless Communication (CWC), University of Oulu, Oulu 90014, Finland.

The upcoming 5G technology is the possible solution to 4G limitations, and by using the institute of electrical and electronics engineers (IEEE) 802.11 protocol, it can enhance the data speed over the air [10]. 5G is a service-enabled platform for consumers, industry, and enterprises with remote e-healthcare, auto manufacturing, online education, IoT, online shopping, and energy utility sectors as shown in Fig. 1. Ericsson is expecting that 40 percent of the global population will be able to access 5G services by the year 2024 and 90 percent population will be covered by 2027 [11]. The deployment from 4G to 5G enabled applications will be determined based on the spectrum allocation, propagation characteristics, and antenna design technology. The 5G spectrum allocation boosts modern wireless communication due to its huge bandwidth [12].

Figure 1. 5G enabled connectivity.

Compared to the 4G network, the 5G system is capable to provide a peak data rate of 20 Gbps and ultra-low latency of 1 millisecond which improves the gaming performance of the device [13]. The key applications of future 5G network communication are depicted in Fig. 2 [14]. Hence, human to human (H2H), human to machine (H2M), and machine to machine (M2M) communication makes 5G technology suitable for modern wireless communication systems. The technical growth of generation is mainly based on technology used, latency, bandwidth, data speed, and channel capacity [15]. For achieving the excellent performance of wireless communication systems, antennas are one of the enabling components of wireless systems with their eminent parameters such as stability in radiation patterns, high data speed, and large bandwidth [16].

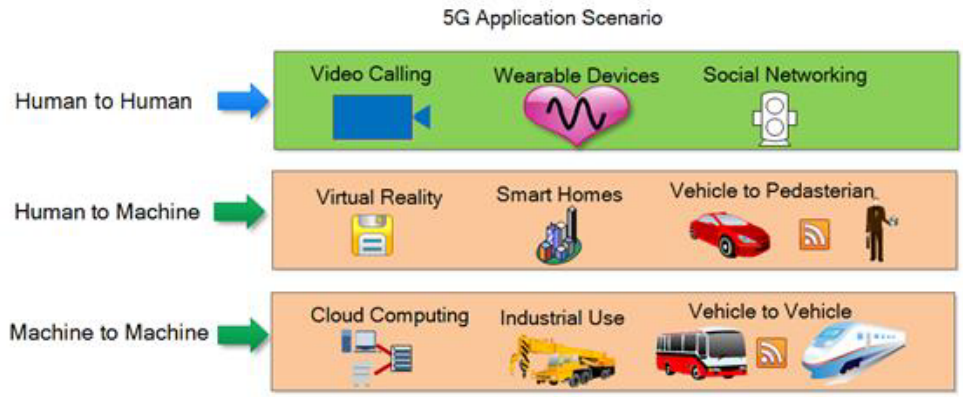

Figure 2. 5G application scenario.

Various antennas are used in 5G wireless communication to achieve their unique behavior such as circular polarization (CP) [17], multiple-input-multiple-output (MIMO) [18], beamforming [19], and beam steering [20]. The well-known mobile industry Xiaomi and Samsung are assembling 5G antennas in mobile phones with long-term evolution (LTE) 4G technology for frequency ranges 2.5 GHz, 3.5 GHz,

and millimeter-wave bands [21, 22]. Thus, rigorous research efforts are carried out on the fundamental of 5G technology, component design, spectrum analysis, and implementation of services. In this paper, various techniques are reviewed to design a 5G antenna with aspects of simulation, optimization, and measurement analysis. The different methods are also analyzed which are responsible for improving the characteristics of an antenna device for the 5G frequency band such as gain enhancement, size reduction, isolation enhancement, and SAR analysis with optimized value. The fabrication process and measurement of the 5G antenna device is another important aspect of mass production [23, 24]. The term "antenna measurements" includes the experimental verification of various parameters such as reflection coefficient, gain, efficiency, and radiation pattern for the antenna-under-test (AUT) [25, 26].

This review paper is structured as follows. Section 2 highlights the spectrum analysis of 5G wireless communication system. Section 3 includes the challenges of 5G mm-Wave technology. Section 4 describes the design consideration and desirable parameters of 5G antennas. It also describes the fabrication process with measurement analysis of various parameters for 5G antennas and recent development in the design techniques. The overall conclusion is summarized in Section 5.

2. 5G SPECTRUM ANALYSIS

According to Federal Communications Commission (FCC), the radio frequency part of the electromagnetic spectrum has been classified as licensed and unlicensed bands. To use a licensed band, the user is required to take the license permission from FCC for significant utilization and free from interference. For high speed and short-range communication, the use of an unlicensed band plays an important role in the real-world scenario that boosts the capacity of 5G communication [27]. Currently, third generation (3G) and 4G bands are congested and over utilized due to the limited bandwidth that limits the data exchange speed. Korea showcased the commercial applications of 5G technology in the winter Olympics Games 2018 at Pyeong Chang and prepared for 5G mass service operations in Seoul and other locations of Korea. Japan adopted new rules for testing the commercial 5G network in the 2020 summer Olympic Games in Tokyo, which were rescheduled for 2021 due to the COVID-19 pandemic. China identified the 26 GHz and 42 GHz bands for commercial 5G networks [28]. United States FCC and European Union (EU) announced 5G pioneer bands as 24.25–27.50 GHz and 27.50–28.35 GHz for 5G broadcasting [29, 30]. Telecom Regulatory Authority of India (TRAI) and the department of telecommunication (DoT) recommended the range 3300 MHz to 3400 MHz, 3425 MHz to 3600 MHz, 24 GHz, and 26 GHz bands for 5G services. The 5G network was partially trialed in 2021 and commercially launched by Ericsson in 2022. The ITU also declared the following frequency band for upcoming 5G communication as 3.4–3.6 GHz, 5–6 GHz, 24.25–27.5 GHz, 37–40.5 GHz, and 66–76 GHz [31].

5G technology spectrum is classified as sub-1 GHz (low-band), sub-6 GHz (mid-band), and mm-Wave band (high-band). The globally accepted 5G spectrum allocation [32] is shown in Fig. 3. In the sub-1 GHz band, the IEEE802.11ah is the current Wi-Fi standard, and it is an alternative to IEEE 802.15 wireless standards. Sub-1 GHz is used to provide wireless access to internet of things (IoT) systems, indoor and outdoor applications, and machine-to-machine (M2M) communication. It provides long-distance communication at a lower frequency to provide coverage across urban, suburban, and rural areas. Similarly, the sub-6 GHz band provides enough capacity and good coverage for wireless mobile communication. The frequency band, ranging from 3.3 to 3.8 GHz, is suitable for various 5G services [33]. High-band including the microwave and millimeter-wave bands ranging from 6 to 100 GHz is the future band of 5G services [34]. The mm-Wave 5G frequency offers a high speed of 20 Gbps [35]. The band of 27.5–28.35 GHz is widely used for 5G services because it is an unused and under utilized band that has low atmospheric absorption. In this band, the rain attenuation and oxygen loss do not increase, and it offers a good propagation constant [36].

The globally accepted 5G frequency spectrum is illustrated in Table 1. 5G new radio (NR) is a new standard for defining the 5G band. It is a new radio air interface that helps to access remote control vehicles with low latency communications. The symbol n is used for a new radio interface that helps to define the band of spectrum and give a common interface across these frequencies. 5G new radio is a future frequency band flourished by the 3rd Generation Partnership Project (3GPP) for mobile telephony. The 700 MHz is the low band for 5G communication with band name n28 and common name

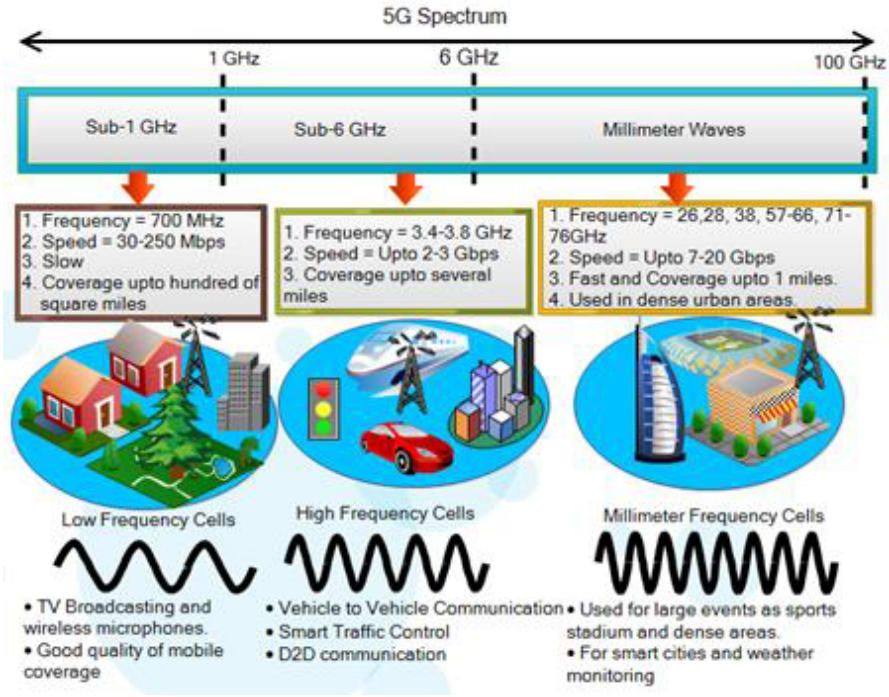

Figure 3. 5G enabled NR spectrum [32].

Table 1. 5G frequency spectrum [37].

Band	Country	Frequency Range (GHz)	Frequency (GHz)	Common Name	Channel Bandwidth (MHz)
n28	USA, China	0.69–0.80	0.7	APT	5, 10, 15
n77	USA	3.30–4.20	3.7	C-band	10, 15, 20, 40, 50, 60, 80, 100
n78	Europe	3.30–3.80	3.5	C-band	10, 15, 20, 40, 50, 60, 80, 100
n79	China	4.40–5.00	4.7	C-band	40, 50, 60, 80, 100
n257	Korea	26.50–29.50	28.0	LMDS	50, 100, 200, 400
n258	Europe, China	24.25–27.50	26.0	K-band	50, 100, 200, 400
n260	Japan	37.00–40.00	39.0	Ka-band	50, 100, 200, 400
n261	USA	27.50–28.35	28.0	Ka-band	50, 100, 200, 400

Asia Pacific Tele community band plan (APT) suitable for long-distance communication. The mid-band is trailed with band names n77, n78, and n79 suitable for several miles distance communication in the US, Europe, China, and SE Asia countries. Future trials for the millimeter-wave bands are planned in Korea, Europe, China, Japan, and the USA with frequencies 26 GHz, 28 GHz, and 39 GHz. The common name of the n257 band is defined as local multipoint distribution in service (LMDS) that is suitable for broadband wireless access under the operating frequency range from 26 GHz to 29 GHz. The millimeter-wave band is the future band for dense and urban areas giving peak data rates from 7 to 20 Gbps [37].

3. CHALLENGES OF 5G MM-WAVE TECHNOLOGY

In the telecommunication industry, mobile communication with smart devices is a more developing segment of wireless cellular systems [38]. The design analysis of the future mm-Wave cellular system

is characterized by a propagation model. The main issues with mm-Wave mobile communication are large path loss, atmospheric attenuation, and signal blockage due to obstacles. Free space path loss (FSPL) is the degradation of the power density of electromagnetic waves. It is directly proportional to the square of the operating frequency of the system. As the operating frequency is increased towards the mm-Wave band, the size of the antenna becomes compact. The effective aperture (A_e) is dependent on wavelength, hence by keeping constant A_e, path loss can be minimized [39]. Another hurdle of mm-Wave frequency band service includes that the attenuation of the signal is due to rain, atmospheric absorption, and foliage. To overcome signal degradation issues and make a mm-Wave frequency band for mobile communication, consider the cell size of the order of 200 meters in urban areas. For a cell size of 200 meters, the atmospheric absorption rate is lower at 28 GHz and 38 GHz and has a significant value at 73–77 GHz. As illustrated in Fig. 4, the atmospheric absorption rate has a peak value from 15 to 30 dB/km at the 60 GHz frequency band [40].

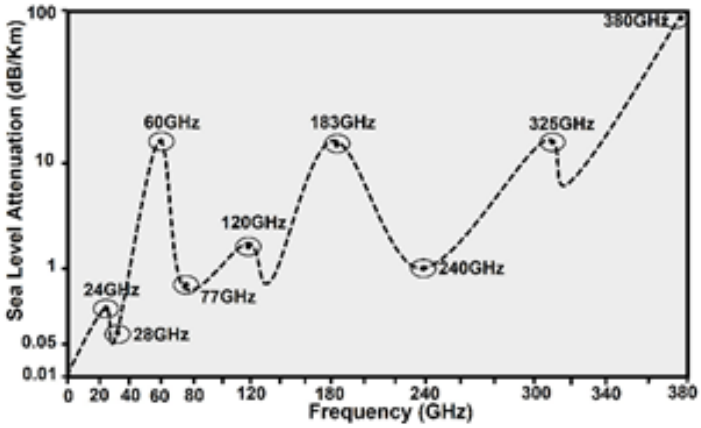

Figure 4. Atmospheric absorption with frequency in dB/km [40].

The efficient spectrum utilization in 5G cellular communication is required for improving data rates, increasing system capacity and reducing latency. D2D communication is the advanced technology for proper utilization of spectral efficiency in future 5G communications. It involves direct communication between nearby mobile devices without using a base station (BS).

The five challenges of D2D communication are illustrated in Fig. 5 [41]. The synchronization is the main challenge in a quick device discovery scheme. Handover is another issue in mode selection and mobility of mobile users. The electromotive force (EMF) level should be in the normal range for proper implementation of 5G communication. At mm-Wave communication, the EMF level may be increased which causes an issue for achieving capacity in the network [42]. For the challenges of

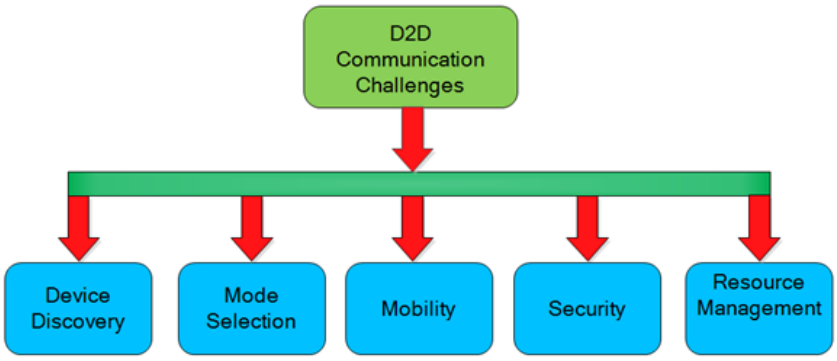

Figure 5. D2D communication challenges in 5G mm-Wave communication [41].

transmitting a volume of traffic, the backhaul mechanism is utilized. The backhaul concept or backbone in cellular communication is the composition of microwave devices, fibers, coppers, and satellites [43]. As comparison with traditional technology, the elements and functions used in 5G communication are virtualized, and resources are shared. Hence, security and reliable communication are the big challenge in mm-Wave 5G communications [44]. The other nontechnical challenges are high cost in terms of infrastructure setup, deployment, and device support criteria. Lack of digital literacy can be a challenge for users as they may not be aware of new services offered by 5G technology.

4. DESIGN CONSIDERATIONS FOR 5G MM-WAVE ANTENNAS

There are several major requirements for generation and revolution of 5G communication technology. For designing the antennas for 5G technology, the researchers are required to have desirable knowledge of propagation model with antenna parameters such as high gain and directivity, efficiency, and wideband operation of upcoming cellular devices.

4.1. Dielectric Substrate for 5G mm-Wave Communication

The mm-Wave frequency band is an eminent candidate for modern mobile communication academically and commercially with industry attention. Fabrication of an antenna is another important aspect that makes it practically available. The substrate selection is also a major challenge in front of researchers for the fabrication of mm-Wave antenna device. There are various parameters such as dissipation loss, moisture absorption, and multi-layered processes for compact device, which are considered for choosing a suitable substrate as shown in Fig. 6.

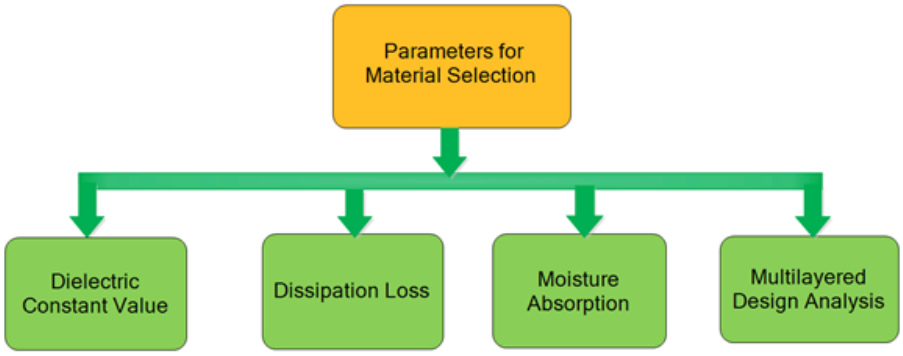

Figure 6. Material selection key parameters for 5G technology [45].

The most important parameter for choosing a substrate material for 5G mm-Wave fabrication is dissipation loss. As going towards higher frequency above 10 GHz, substrate loss becomes dominant and scales with loss tangent $\tan\delta = \sigma/(\omega * \varepsilon)$. Hence, the material substrate with minimum value of loss tangent will be useful for building an mm-Wave antenna. The other impediment for material selection is moisture absorption which becomes a driving parameter at high frequency. The absorption of water by material affects the antenna performance and changes the dielectric constant. The dielectric substrate with high water absorption enhances the loss of the antenna. At mm-Wave frequency multi-layered structures become the backbone to design a compact antenna with wide and multiple bands. The fabrication of a multi-layered structure is possible by choosing a suitable substrate for mm-Wave antennas [45]. As the frequency increases towards mm-Wave range, the wavelength and size of antenna shrink. Hence, researchers consider the material with low dielectric constant values for the reliable performance of antenna, typically around 2 to 4 or an average of 3. The comparison of various substrate materials with parameters is illustrated in Table 2 [46–49]. From Table 2, it is analyzed that FR-4 is rolled out for mm-Wave frequency band due to its characteristics as water absorption rate and dissipation factor are high as compared to low dielectric value substrate. RT Duroid 5880 is the best suitable material for the fabrication of mm-Wave antennas.

Table 2. Comparison of substrate used for 5G technology [46–49].

Property	RT Duroid 5880	RT Duroid 5870	Rogers RO3003	Rogers RO4003	Rogers RO4350	FR-4 Epoxy
Dielectric Constant (ε)	2.2	2.33	3.0	3.55	3.66	4.4
Dissipation Factor (tanδ)	0.0009	0.0010	0.0010	0.0027	0.0037	0.025
Moisture Absorption (%)	0.02	0.02	0.04	0.06	0.06	0.1
Thermal Conductivity (W/m-K)	0.20	0.22	0.50	0.71	0.69	0.81

4.2. Millimeter-Wave Antenna Design Analysis

The communication between two or more devices without physical wires in the propagation path is called wireless communication. In future era, wireless data traffic will be exponentially increasing because of increasing the number of mobile devices such as smart phones, laptops, tablets, and other devices. Wireless communication has many benefits as compared to wired system due to easy carry of the device anywhere and becomes popular for future 5G communication. To fulfil the requirements such as ultra-low latency, data rate of 1–10 Gbps, large bandwidth, etc. of 5G wireless technology, various efficient antennas have been reported. High gain can be achieved by using antenna array techniques to overcome signal fading issue due to poor weather condition in both line-of-sight (LOS) and non-line-of-sight (NLOS) communication [50]. Wideband and multiband operation can be achieved by frequency reconfiguration mechanism. An arrangement of 5G mm-Wave antenna with LOS communication is capable to provide low latency, good battery life, high spectral efficiency, and faster connectivity. Latency is the time taken during transmission of signal and eminent parameter for online games, video streaming, and multimedia [51]. Device battery life is also a significant aspect for 5G communication as mm-Wave cell size is small, so less transmitted power is required than currently used base station [52].

The major limitation of wireless communication at mm-Wave frequency is multipath fading due to NLOS propagation. The NLOS propagation occurs due to physical obstacles as tall building, trees, and dense areas. Single antenna is not feasible at mm-Wave frequency. The multiple-input-multiple-output (MIMO) techniques were the remedial by using more than one antenna at transmitter and receiver. Massive MIMO technique with 64–256 antennas offers data speed more than ten times of current 4G networks. The multipath propagation is caused by walls and ground surface which can be minimized by using circularly polarized antennas in modern communication systems [53]. The antenna design analysis with different parameters is explained as follows.

4.2.1. High Gain mm-Wave Antennas

In present scenario, to resolve signal fading problem due to poor weather condition, high gain antenna design become the interest of research community. Several methods such as antenna arrays, multilayered structure, substrate integrated waveguide (SIW) cavity, and artificial metamaterial as artificial magnetic conductor (AMC) are reported to achieve high gain and directivity. AMC is an artificial metamaterial which acts as reflector to enhance the characteristics of antenna. A 3×3 series-fed patch antennas array is reported for 28 GHz mm-Wave applications [54], in which the patches are connected in series with high impedance microstrip lines as shown in Fig. 7, and using 4 ports, a good gain of 15.6 dBi is obtained.

In [55], a broadband printed-dipole antenna with 8-elements array is reported for 5G application. The presence of an 8-element array results in the peak gain of 12.5 dBi over the operating frequency band of 26–40 GHz range depicted as in Fig. 8. The reported magneto-electric (ME) dipole antenna is

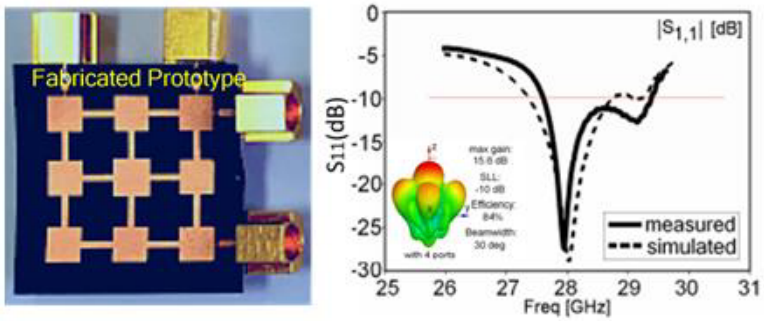

Figure 7. (a) Fabricated prototype (3×3 antenna array), (b) $|S_{11}|$ plot [54].

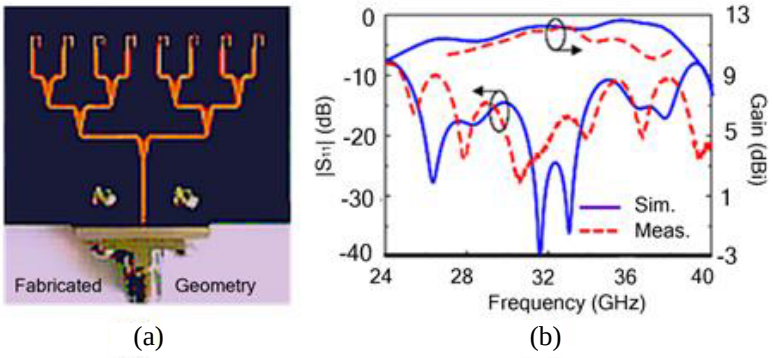

Figure 8. (a) Fabricated design (8-element array), (b) $|S_{11}|$ and gain plots [55].

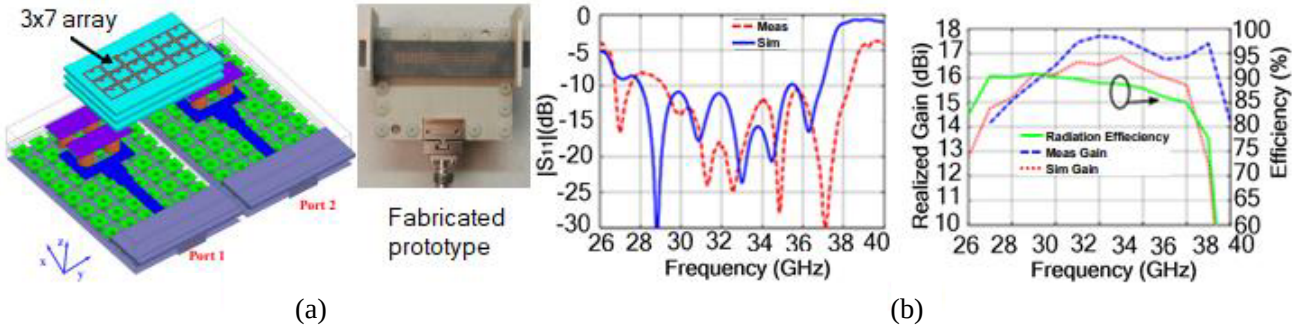

Figure 9. (a) Schematic of ME dipole antenna with SRR cells, (b) S_{11}, gain and efficiency plots [56].

excited by a slot coupled with a fork-shaped printed ridge gap waveguide line, and -10 dB bandwidth is achieved from 26.5 to 38.8 GHz. By using a meta-lens with three layers of 3×7 arrays of split ring resonators (SRRs) integrated in front of a ME dipole antenna as illustrated in Fig. 9, the peak gain of antenna varies from 16.7 to 17.6 dBi over the frequency bandwidth of 29.1–37.8 GHz [56].

Various antenna arrays based on microstrip lines are investigated. However, microstrip lines are significantly used in antenna arrays design because of its easy fabrication and low cost, but not suitable for mm-Wave frequency band. The limitations of microstrip lines at higher frequencies are transmission loss and undesired radiations. SIW is an attractive choice to solve problem and acts as a bridge between planar and non-planar structures. Basically, the SIW cavity is developed in simulation design by metallic vias and consecutive center to center distance.

In [57], a wideband unequal feeding network with an SIW antenna array is designed at 28 GHz

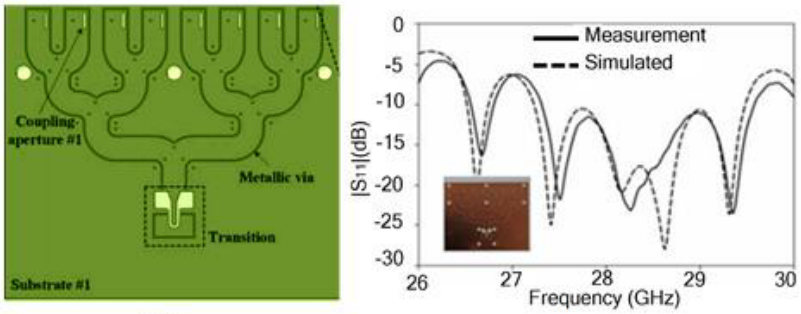

Figure 10. (a) Geometry of SIW antenna array, (b) $|S_{11}|$ plot [57].

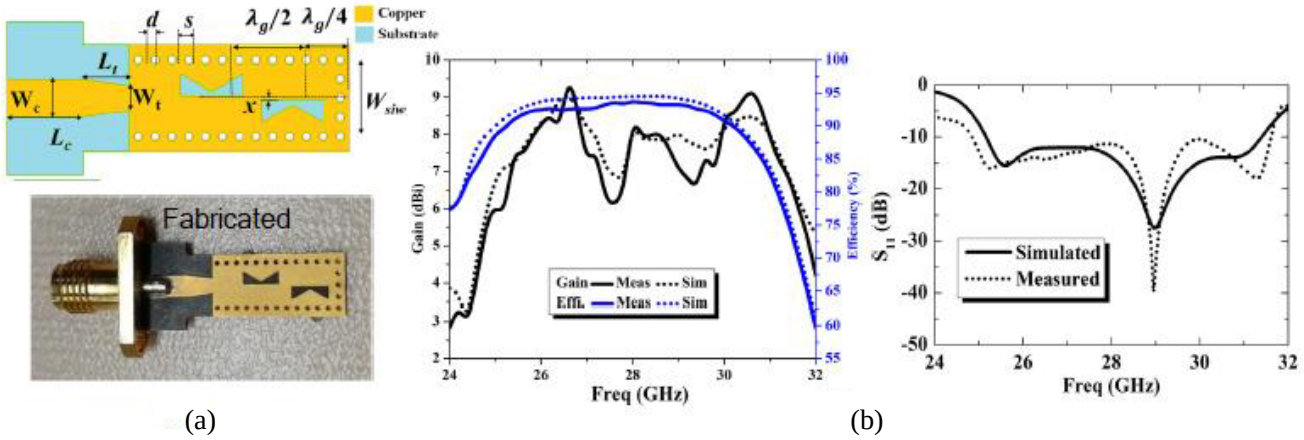

Figure 11. (a) Geometry of wideband SIW slot antenna, (b) gain with efficiency and $|S_{11}|$ plots [58].

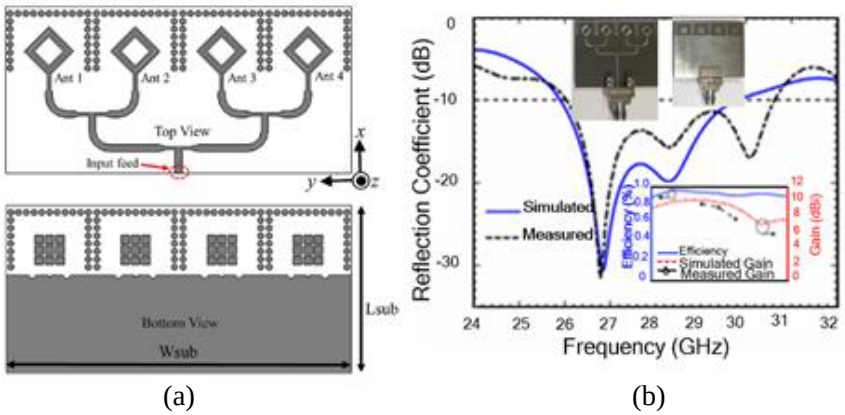

Figure 12. (a) Geometry of rhombus antenna array, (b) $|S_{11}|$ and gain with efficiency plots [59].

frequency band for handset device as shown in Fig. 10. In [58], the authors demonstrated a compact dual mode wide band antenna for 5G mm-Wave applications as shown in Fig. 11. By using SIW technique with two element arrays of half bowtie slots, a wide impedance bandwidth of 6.8 GHz (24.8–31.6 GHz) and peak gain of 8.5 dBi are achieved as illustrated in Fig. 11. In [59], a rhombus shaped monopole 4-element antenna array for 28 GHz is reported as depicted in Fig. 12. It has the size of $40 \times 19.22 \times 0.254\,\text{mm}^3$. Wide operating frequency band is obtained using a DGS (defected ground

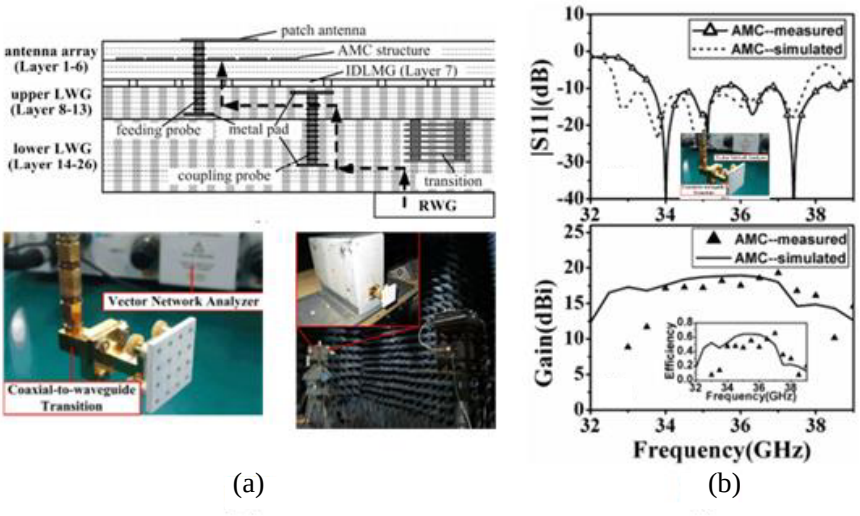

Figure 13. (a) Geometry of mm-Wave LTCC antenna array, (b) $|S_{11}|$ and gain plots [60].

Table 3. Summary of high gain antennas.

Ref.	Techniques Used	Impedance B.W. (GHz, %)	Peak Gain (dBi)	Efficiency (%)	Size (mm^2)
[54]	3×3 Series Feed Planar Array	27.48–28.63, 4.09	15.6	> 85	20×20
[55]	8 Element Linear Array	26.50–38.20, 36.20	12.5	> 93	—
[56]	Multilayer Design	26.50–38.80, 36.4	17.6	> 90	38×27
[57]	SIW Cavity	27.20–29.50, 8.11	14.9	> 75	70×63
[58]	SIW Slot Antenna	24.80–31.60, 24.0	8.50	> 90	—
[59]	SIW Cavity	26.04–30.63, 16.20	11.24	> 85	40×19.22
[60]	AMC array structure	33.65–38.70, 13.96	19.10	> 63	26×26
[61]	SIW Antenna Array	27.0–29.0, 7.14	17.30	> 85	66.7×47.5

structure) in the bottom side of array antenna. By using an antenna array with a simple feed network, a peak gain of 11.24 dBi and more than 85% efficiency are achieved. A low-temperature co-fired ceramics (LTCC) antenna with AMC array is demonstrated. By designing a multilayer laminated waveguide (LWG) power divider with an array, a stable high gain of 19.1 dBi and 63.1% efficiency are achieved over the wide operating frequency band (i.e., 34–37 GHz). The design topology and results are depicted in Fig. 13 [60]. By using their properties such as in-phase reflection and high impedance surface, the AMC acts as a reflector and enhances the radiation characteristics of antenna device. The summary of cited high gain antennas [54–61] is illustrated in Table 3.

4.2.2. High Isolation mm-Wave Antennas

Generally, single antennas are not feasible due to NLOS communication network. The limitations of single RF antenna are poor reliable communication, path loss attenuation, and signal fading. MIMO technique is a future solution for 5G communications and enhances the performance of antenna in terms of gain, efficiency, data rate, and capacity of system without any additional spectrum. In MIMO systems, multiple antennas are designed by placing near each other and used to transmit the signals simultaneously. By placing the radiating metal patches or antenna elements at less than $\lambda/4$

distance in the same plane, the high mutual coupling is created. It is defined as the interaction of electromagnetic field between antenna elements [62]. In antennas, mutual coupling is observed due to the shared ground effect and between antenna elements. The high correlation and high mutual coupling reduce the performance of a MIMO antenna system. The term coupling is inversely related to the isolation and can be calculated using scattering parameters, which is defined as $I = -10\text{Log}_{10}|S_{ij}|$, where i and j are related to the port used. To analyze the diversity for MIMO antenna, numerous parameters such as envelope correlation coefficient (ECC), diversity gain (DG), total active reflection coefficient (TARC), and channel capacity loss (CCL) are considered [63]. ECC (ρ) is an important term that describes how the antennas are isolated from each other in a communication system. If one antenna is vertically polarized, the other antenna should be completely horizontally polarized, then ECC will be zero between antennas. ECC will be calculated as using S-parameters by Equation (1) [64, 65].

$$\rho_{eij} = |\rho_{eij}|^2 = \left| \frac{S_{ii}S_{ij}^* + S_{ji}S_{jj}^*}{|(1 - S_{ii} - S_{ji})(1 - S_{jj} - S_{ij})|^{1/2} \eta_{rad_i}\eta_{rad_j}} \right|^2 \tag{1}$$

where ρ_{eij} is the envelop correlation coefficient, ρ_{ij} the correlation coefficient, S_{ij} the coupling parameter between i and j elements, and η_{rad_i} and η_{rad_j} are the radiation efficiency factors for i and j elements, respectively.

The MIMO antenna system provides good diversity performance by having high isolation and low correlation coefficient. For good diversity, the acceptable ECC value is $\rho = 0.5$ for mobile antenna system, if the ECC is greater than 0.5 that means system is uncorrelated. For MIMO antenna, the DG is another important parameter that gives diversity performance. The DG and ECC are related with each other as given by Equation (2) [66]. The lower the value of ECC is, the greater the diversity gain of MIMO antennas will be and vice versa.

$$\text{DG} = 10 * \sqrt{1 - |\rho|^2} \tag{2}$$

TARC is another very useful characteristic in MIMO antenna to obtain an effective operational bandwidth. It is dependent on ECC and magnitude of S-parameter. For a MIMO antenna system, TARC is the ratio of the square root of total reflected power to the square root of total incident power [67]. The formula of TARC for N port antenna can be written as in Equation (3).

$$\Gamma_a^t = \frac{\sqrt{\sum_{i=1}^{n} |b_i|^2}}{\sqrt{\sum_{i=1}^{n} |a_i|^2}} \tag{3}$$

where a_i is the excitation vector, and b_i is the scattering vector.

CCL is also a very important parameter to explain the performance of MIMO antenna in a scattering environment. It is used to measure the performance of MIMO antenna in terms of number of bits transmitted per Hz of the bandwidth during the correlation. The formula for CCL calculation is given by Equations (4), (5), (6), and (7) [68].

$$c_{\text{Loss}} = -\log_2 \det\left(\psi^R\right) \tag{4}$$

$$\left(\psi^R\right) = \begin{bmatrix} \rho_{11} & \rho_{12} \\ \rho_{21} & \rho_{22} \end{bmatrix} \tag{5}$$

$$\rho_{ii} = 1 - |S_{ii}|^2 - |S_{ij}|^2 \tag{6}$$

$$\rho_{ij} = -(S_{ii}^* S_{ij} + S_{ji}^* S_{ij}) \tag{7}$$

Consider i, j = (1 or 2). Basically, the value of CCL for MIMO antenna must be less than 0.5 bits/s/Hz.

Various MIMO antennas have been reported for high isolation and low mutual coupling in the literature. In [69], a CPW-fed systematic T-shaped DGS based MIMO antenna is depicted in Fig. 14(a)

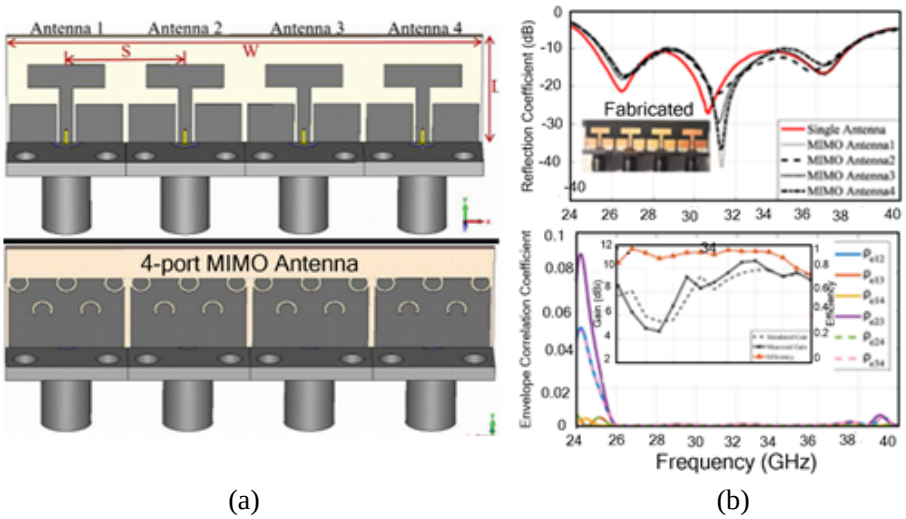

Figure 14. (a) Geometry of four-element mm-Wave MIMO antenna, (b) antenna results [69].

at mm-Wave spectrum for 5G applications. It has the size of 12 mm × 50.8 mm. Fig. 14(b) illustrates the reflection coefficient plot with fabricated model, gain, and ECC plot of antenna with and without DGS. By using five split-ring slots in bottom ground plane as DGS, it provided a wideband of 12.4 GHz (25.1–37.5 GHz) bandwidth at mm-Wave frequencies.

Mew SIW corrugated technique based MIMO antennas (namely MIMO 1 and MIMO 2) were demonstrated for Ka-band. By using isolation vias between every two elements, more than 20 dB isolation and ECC value of less than 0.0002 are achieved for both MIMO antennas. The sizes of MIMO 1 and MIMO 2 antennas with SIW groove are 72 mm × 17.2 mm and 39.98 mm × 33.4 mm, respectively. In Fig. 15, the fabricated prototype of mm-Wave MIMO antennas and their $|S_{11}|$ with ECC results are presented [70].

A four-port MIMO array with the overall dimension of 30 mm × 35 mm excited by the feed network has been reported for mm-Wave 5G communication. The reported MIMO antenna operated in the frequency band of 26.1–30.0 GHz with 13.9% fractional bandwidth. By employing polarization diversity

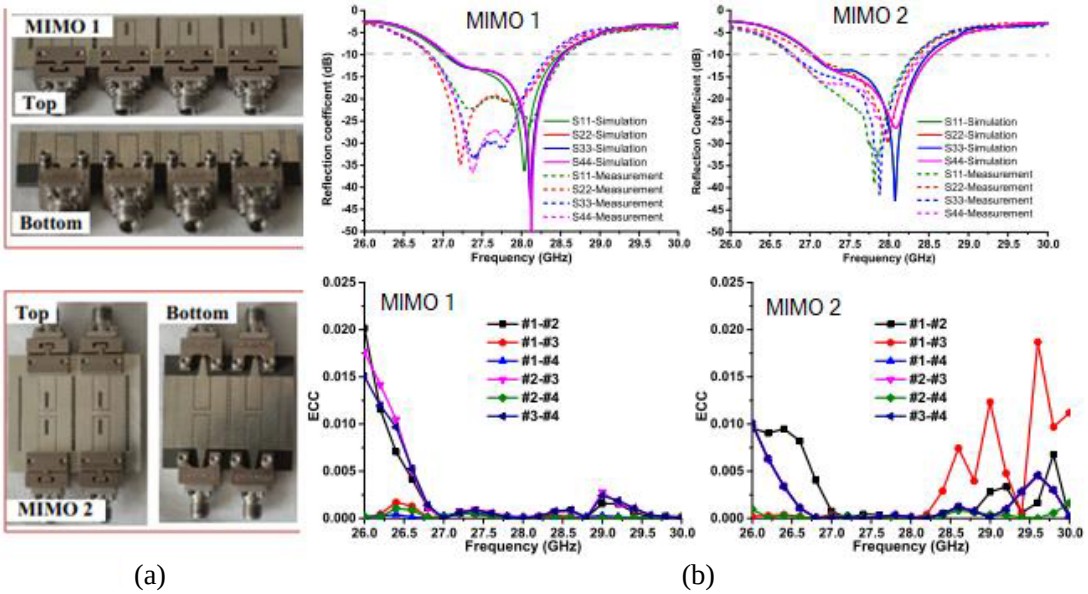

Figure 15. (a) Fabricated prototype of mm-Wave MIMO antennas, (b) $|S_{11}|$ and ECC results [70].

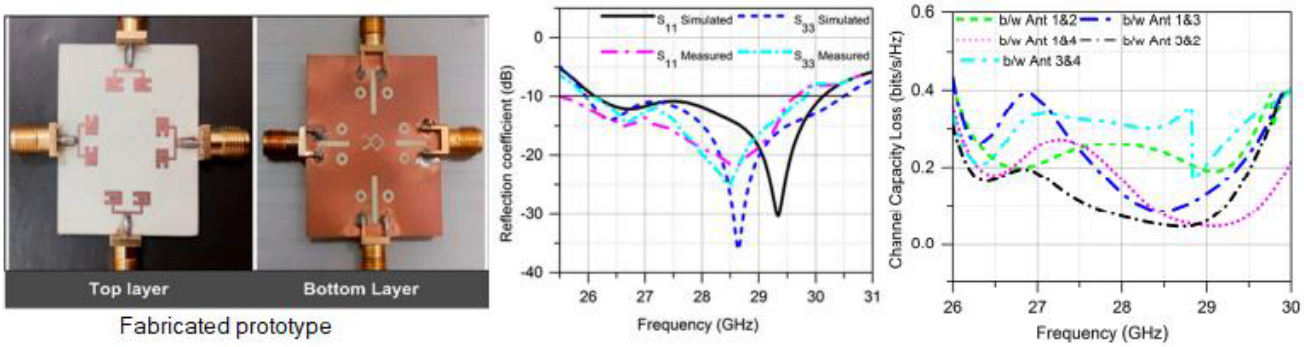

Figure 16. Fabricated prototype of mm-Wave MIMO antenna and their results [71].

between the adjacent radiators, a good isolation of more than 17 dB is realized. The channel capacity loss is obtained less than 0.4 bit/s/Hz over the operating frequency band. In Fig. 16, the fabricated design and its results are illustrated [71].

The summary of cited [69–77] high isolation antennas is depicted in Table 4. From Table 4, it is examined that mostly researchers use low permittivity dielectric material for designing of mm-Wave antennas.

Table 4. Summary of high isolation mm-Wave antennas.

Ref.	Antenna Type	Impedance B.W. (GHz, %)	Substrate Used	Isolation (dB)	ECC (ρ)	Efficiency (%)
[69]	T-shaped DGS MIMO antenna	25.10–37.50, 39.68	Rogers 5880	> 22	< 0.010	> 80
[70]	SIW MIMO Antenna	26.80–28.40, 5.80	Rogers 5880	> 20	< 0.02	—
[71]	MIMO Antenna with DGS	26.10–30.00, 13.90	Rogers 4350	> 17	< 0.04	> 82
[72]	DRA MIMO Antenna	27.25–28.59, 4.80	Rogers 5880	> 24	< 0.013	—
[73]	Four-port MIMO Antenna	23.00–29.00, 23.0	Rogers 5880	> 28	< 0.0002	—
[74]	Switched Beam Antenna	27.40–28.23, 2.98	RO3003	> 18	< 0.0008	—
[75]	Metallic Based Dipole Antenna	26.00–31.00, 17.50	Neltec	> 21	< 0.0015	—
[76]	Tapered Slot Antenna	27.00–32.00, 16.90	RO4003	> 37.1	—	—
[77]	Annular Slot MIMO Antenna	27.80–28.20, 1.40	TLY-5	> 30	< 0.065	—

From the study it is perceived that to reduce the mutual coupling and isolation enhancement of the MIMO antennas, various techniques such as antenna placement and orientation approach, significant gap between antenna elements, isolation vias, protruding ground stub structures, meandered line, parasitic elements, etching slot and slit elements, neutralization lines, electromagnetic bandgap structures, metamaterial structure, decoupling networks, and DGS can be employed [69–79]. These techniques are also helpful for achieving low ECC value, high diversity performance, and multiband operation of MIMO antennas.

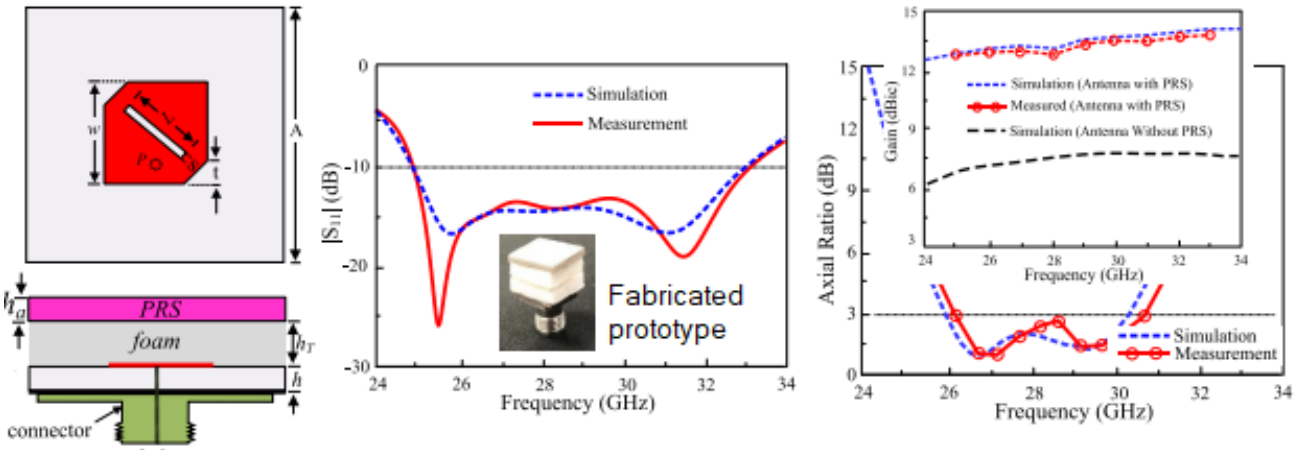

Figure 17. (a) Geometry of Fabry-Perot antenna, (b) simulated and measured $|S_{11}|$ and axial ratio [81].

4.2.3. Circularly Polarized mm-Wave Antennas

The polarization of antenna plays an important role in installation process as well as in selection of antennas. The strength of signal will be maximum between antennas when transmitting and receiving antennas are properly aligned and having identical polarization. The selection of antenna is taken into consideration based on polarization such as linear or circular polarization.

The circularly polarized antennas are useful for resolving multipath propagation in modern communication systems. A CP wave is described by the orientation of E-vector. It can be classified as right-hand circular polarization (RHCP) wave and left-hand circular polarization (LHCP) wave. The LHCP wave is generated when the rotation of E-vector is counterclockwise, and for RHCP wave the rotation direction of E-vector is clockwise [80]. Axial ratio (AR) is the measure of circularly polarized nature of the antenna. For CP antenna, AR is 0 dB ideally but practically less than 3 dB is considered.

A low profile, compact size, and broadband circularly polarized Fabry-Perot resonant antenna with single layer partially reflected surface (PRS) is presented for future 5G applications [81]. By stacking PRS on radiating patch, a wideband of 25–33 GHz (27.6%) and stable gain of 14.10 dBi are achieved. The corner cut patch with diagonal slot is useful for getting circular polarization and provided 17% (26–31.3 GHz) wide 3-dB ARBW. The geometry of the Fabry-Perot antenna and its characteristics are illustrated as in Fig. 17. A single-feed broadband CP antenna is reported for mm-Wave frequency band [82]. An Archimedean spiral radiator is coupled with a specially shaped ring-slot structure at the bottom layer to obtain circular polarization and bandwidth improvement. It has compact size of 30 mm × 15 mm and etched on a Roger5880 substrate with thickness of 0.254 mm. It has −10 dB impedance bandwidth of 21.10–34.10 GHz (46.43%) and 3-dB ARBW of 23.8–32.20 GHz (29.82%). The geometry of Archimedean spiral patch CP antenna and its radiation characteristics are shown as in Fig. 18.

In [83], a broadband circularly polarized T-shaped monopole antenna with an inverted L grounded stub and coplanar waveguide (CPW) feed is reported for mm-Wave short range 5G communications. The inverted L-grounded stub is embedded with a horizontally T-shaped patch radiator to realize circular polarization. The mm-Wave CPW-fed monopole antenna is designed on an RO4003 dielectric substrate ($\varepsilon_r = 3.55$) with the thickness of 60 mil (1.524 mm). The impedance bandwidth of 25.6–33.9 GHz (27.9%), 3-dB ARBW of 27.26–31.26 GHz (13.67%), and peak gain of 7.15 dBi are presented. The geometry of the monopole antenna and its results are depicted in Fig. 19. The summary of cited circularly polarized state-of-the-art mm-Wave antenna works [81–96] are illustrated in Table 5.

Table 5. Summary of various circularly polarized state-of-the-art mm-Wave antennas.

Ref.	Antenna Type	IBW (GHz, %)	3-dB ARBW (GHz, %)	Gain (dBi)	Polarization	Antenna Size ($\lambda_L \times \lambda_L$)
[81]	Fabry-Perot Antenna	25.0–33.0, 27.60	26.0–31.30, 17.0	14.1	LHCP/RHCP	1.58×1.58
[82]	Spiral Patch Antenna	21.10–34.10, 46.43	23.8–32.2, 29.82	6.49	LHCP/RHCP	2.10×1.05
[83]	CP Monopole Antenna	25.60–33.90, 27.90	27.26–31.26, 13.67	7.15	LHCP/RHCP	1.87×1.70
[84]	Parasitic Patch Antenna	22.8–33.8, 35.97	28.77–33.5, 15.19	5.2	LHCP/RHCP	0.43×0.50
[85]	End-fire CP Antenna	32.00–43.00, 29.30	33.5–42.0, 22.50	12.8	LHCP/RHCP	—
[86]	SIW Antenna Array	27.40–28.95, 5.50	27.7–28.8, 3.8	13.09	LHCP/RHCP	6.39×5.80
[87]	Helical Antenna Array	26.5–40.0, 41.0	27.0–39.0, 36.0	9.50	LHCP/RHCP	1.33×2.21
[88]	Compact CP Antenna	27.00–28.50, 5.0	25.7–28.5, 10.0	2.2	RHCP	0.31×0.31
[89]	Stack Patch Antenna	26.30–33.40, 23.80	27.20–30.70, 11.60	6.9	CP	0.79×0.79
[90]	FSS Polarizer Antenna	28.0–34.0, 19.30	26.0–30.5, 16.0	9.0	CP	2.43×0.84
[91]	SIW End-Fire Antenna	22.0–27.0, 20.0	24.25–26.50, 9.0	8.0	LHCP/RHCP	—
[92]	Waveguide Slot Antenna	31.51–39.21, 21.7	31.72–38.53, 19.38	9.08	LHCP	1.06×3.36
[93]	CP Waveguide Antenna	26.85–32.85, 20.0	28.80–32.85, 13.50	9.39	RHCP	0.78×0.92
[94]	CP Antenna Array	27.0–38.0, 33.8	29.2–30.7, 5.0	9.50	LHCP/RHCP	2.0×2.0
[95]	ME Dipole Antenna	24.1–31, 24.6	25–30, 18.1	8	RHCP	0.83×0.83
[96]	Dipole Antenna Array	26.26–34.71, 27.7	27–36, 28.5	17.85	RHCP	—

4.2.4. Reconfigurable mm-Wave Antennas

In modern era communication, the wireless devices need a smart antenna with different functional properties such as beamforming, beam-steering, imaging, and direction finding in radar communication [97]. To achieve the desired operating characteristics, a reconfigurable antenna is required. The reconfigurable antenna performs multiple functions with only a single antenna structure rather than using multiple antennas. The characteristics of an antenna can be changed by using two or more discrete or continuous switchable states that changes the current path of antenna [98]. The reconfigurable mechanism changes frequency resonance, radiation pattern, and polarization of

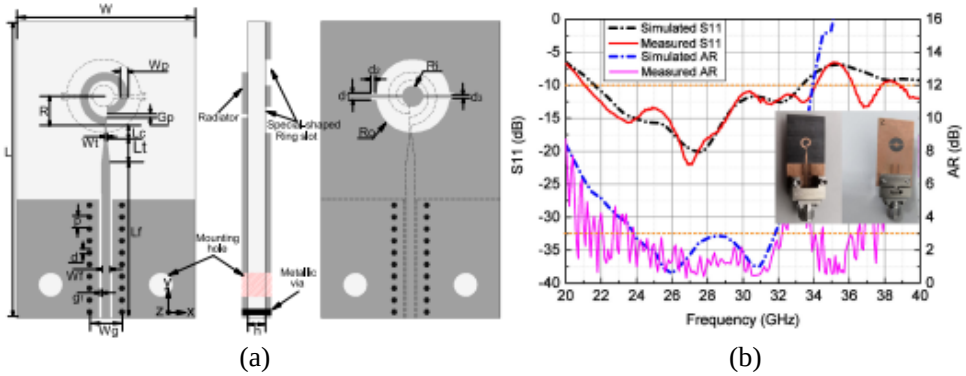

Figure 18. (a) Geometry of spiral patch CP antenna, (b) $|S_{11}|$ and AR results [82].

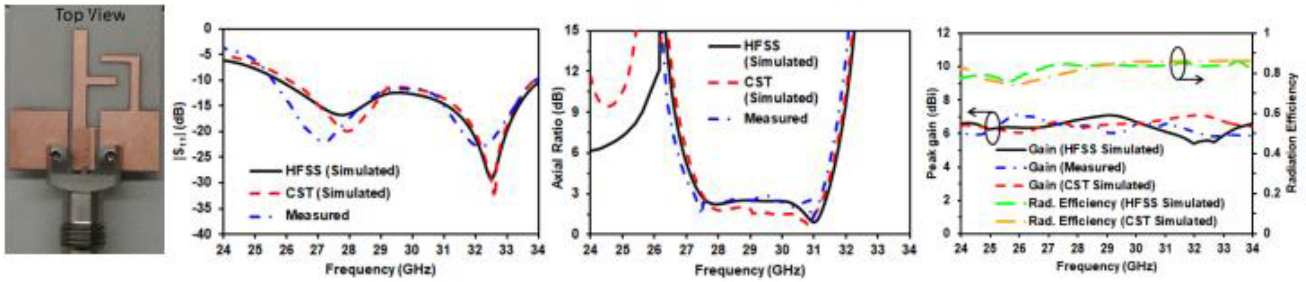

Figure 19. Fabricated prototype of CPW-fed monopole antenna and their results [83].

antenna. They can be designed using single antenna element or in the form of an antenna array. Major reconfigurable techniques are classified as electrical reconfiguration, material reconfiguration, optical reconfiguration, and physical reconfiguration as shown in Fig. 20. The electrical reconfiguration antennas are designed using PIN diode, RF MEMS, and varactor diode. Material selection is very important to achieve reconfigurability in antennas. It can be solid ferrite and ferroelectrics, liquid crystal, and liquid dielectric substrates.

The concept of reconfiguration was used first time in the early 1930's. In [99], a two-element array steered by using a mechanically variable phase changer to study the direction of incoming signal is presented. A corner truncated square patch antenna is demonstrated for mm-Wave communications [100]. The polarization reconfiguration is achieved by using independently biased PIN diodes D1 and D2. By switching diodes D1 and D2 as ON or OFF states, the LHCP and RHCP behavior of the antenna is presented. By using a T-junction with two arms feeding mechanism, the simulated impedance bandwidth and axial ratio of 27.6–28.6 GHz and 27.65–28.35 GHz are attained, respectively, as depicted in Fig. 21.

Radio-frequency micro-electro-mechanical-system (RF MEMS) switches are new generation devices that are useful for performing the operation from microwave frequencies to mm-Wave frequencies. RF MEMS switches have better performance than PIN diode up to 40 GHz frequency band in terms of isolation, power consumption, and insertion loss. Brown introduced the first reconfigurable RF-MEMS antenna systems in 1998 [101]. A CPW-fed pattern reconfigurable antenna with RF MEMS switches for Ka-band is presented in Fig. 22 [102]. The reported antenna consists of one driven patch, two parasitic patches, and two MEMS switches. By changing the states of MEMS switches, a reconfigurable radiation pattern is obtained. The reconfigurable antenna operates in four modes as RF switches change the current phase of adjacent elements. It resonates at 34.9 GHz, 35.4 GHz, 34.5 GHz, and 35.2 GHz frequencies. The measured gains in maximum radiation direction in all the four modes are 5.78 dBi, 6.49 dBi, 7.24 dBi, and 6.31 dBi, respectively.

Varactor diodes are another choice to achieve continuous tuning. A fabricated prototype slot antenna is demonstrated shown in Fig. 23 for mm-Wave band [103]. The varactor diodes are used to

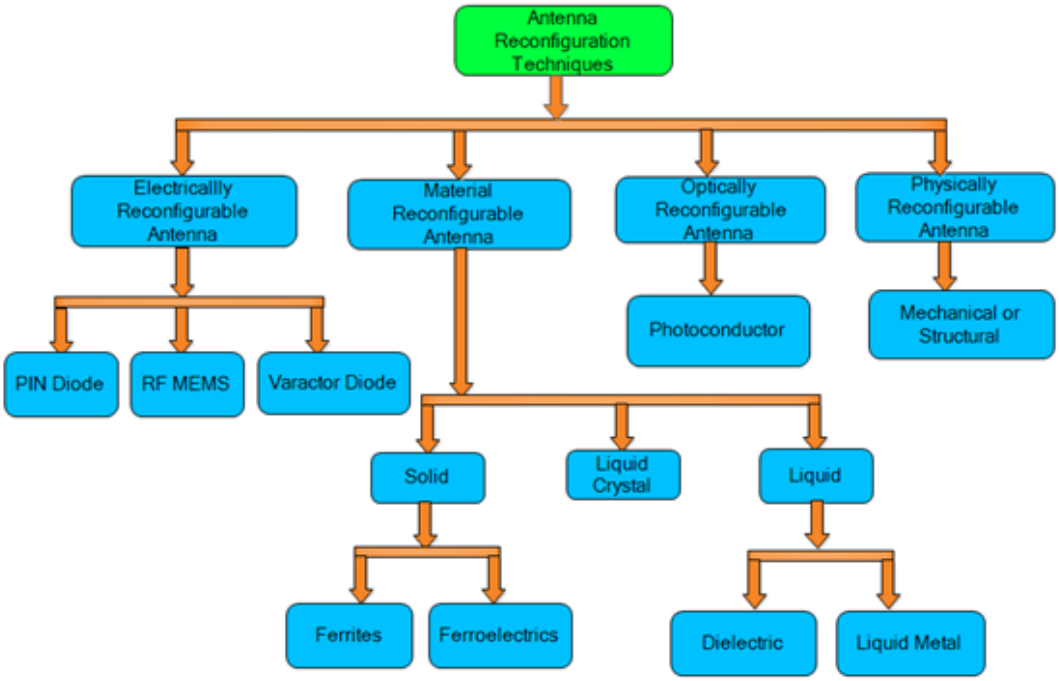

Figure 20. Antenna reconfiguration techniques [98].

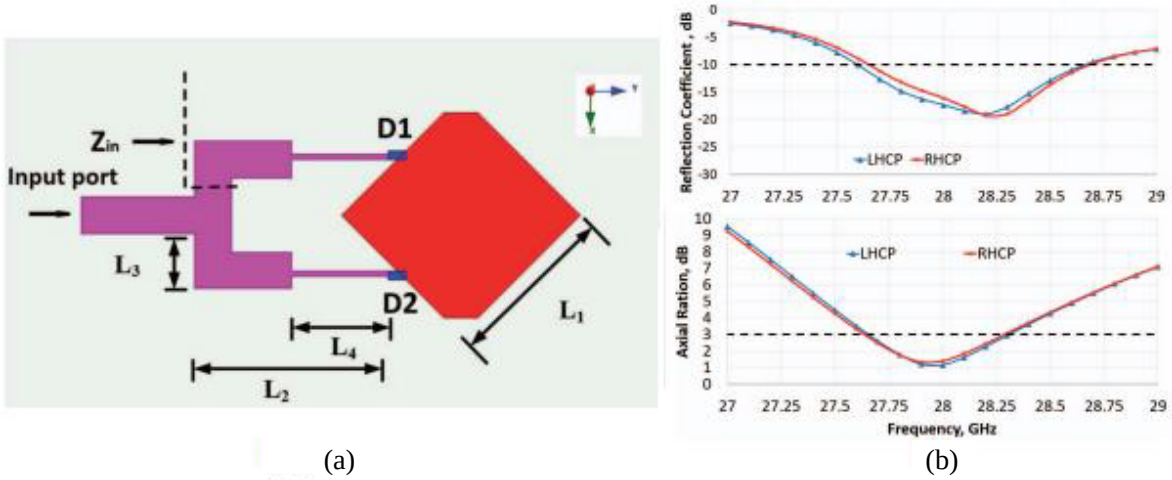

Figure 21. (a) Geometry of truncated square patch antenna, (b) $|S_{11}|$ and axial ratio results [100].

achieve frequency tunability. By using 8 periodic feeders with connected slot antenna array (CSAA), a -10 dB impedance bandwidth of 23–29 GHz and peak gain of 12.5 dBi are achieved. The overall antenna has the size of $70 \times 60 \times 0.381\,\text{mm}^3$. The summary of cited [100, 103–107] reconfigurable antennas is illustrated in Table 6. After studying various cited articles, the pros and cons of mm-Wave switches are summarized in Table 7.

Therefore, electrically reconfigurable techniques are more popular and widely used in antennas. PIN diodes have faster switching around 1–100 nsec. The RF MEMS switches offer low switching speed as compared to PIN diode and provide good isolation. Both PIN diode and RF MEMS switch offer discrete tuning. Varactor diodes are also used in designing various reconfigurable antennas due to its continuous tuning. Various smart materials, liquid crystals, ferrites, and ferroelectrics are used to make reconfigurable antennas. Liquid metal based reconfigurable antennas are useful for sensors and wearable electronic devices.

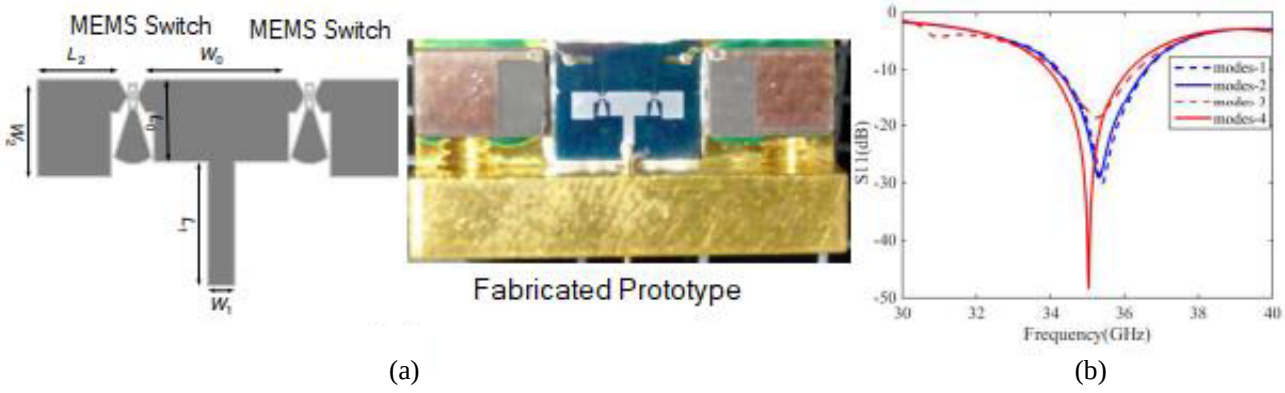

Figure 22. (a) Geometry of reconfigurable antenna with RF MEMS switches, (b) $|S_{11}|$ plot [102].

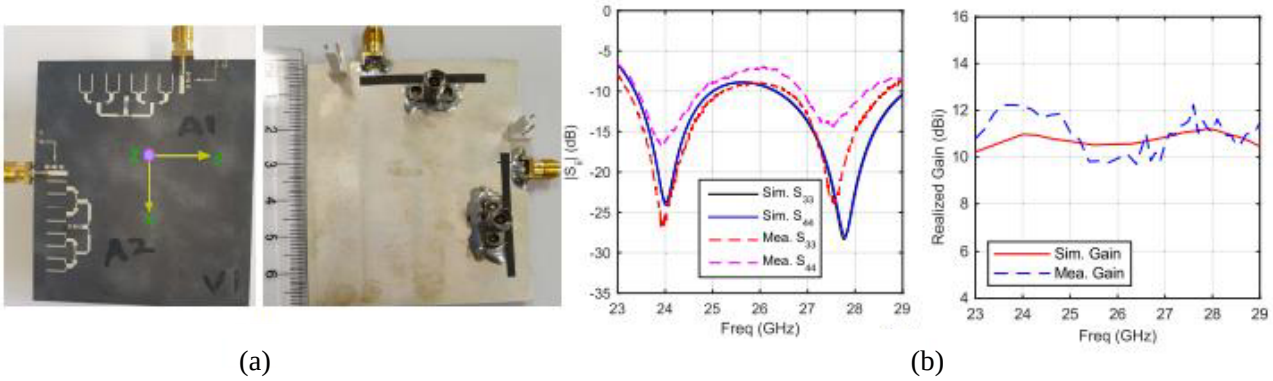

Figure 23. (a) Fabricated prototype of reconfigurable antenna with varactor diode, (b) $|S_{11}|$ and gain plots [103].

Table 6. Summary of various cited mm-Wave reconfigurable antennas.

Ref.	Antenna Type/ Reconfiguration Techniques	IBW (GHz)	Reconfiguration Type	Gain (dBi)	Efficiency η (%)	Substrate Used
[100]	Truncated Square Patch/PIN Diode	27.60–28.60	Polarization	7.20	—	RT Duroid 5880
[103]	Slot Antenna Array/ Varactor Diode	2.05–2.70, 23.0–29.0	Frequency	12.5	> 80 > 85	RT Duroid 5880
[104]	CPW Fed Bowtie Antenna/RF MEMS	24.30–32.20	Frequency	—	—	Si Wafer, Cu or Au
[105]	Patch Antenna	16.80–28.40	Frequency	—	> 27	RT Duroid 5880
[106]	T-shaped Patch Antenna	23.00–29.00	Frequency	—	—	RT Duroid 5880
[107]	Stacked Patch Antenna Array	25.20–33.90	Pattern	19.2	> 80	RO 3003
[108]	Antenna Array	27.2–28.35	Polarization	6.0	> 51	RT Duroid 5880

Table 7. Pros and cons of different mm-Wave switches [109–113].

Switch Types	Pros	Cons
PIN diodes	1. Faster switching speed	1. High D.C. bias
	2. Low cost	2. High tuning speed
RF MEMS	1. High isolation	1. Slow switching speed
	2. Low power loss	2. High control voltage
	3. Wide impedance bandwidth	3. Limited life cycle
Varactor diode	1. Ease of integration	1. Non-linearity
	2. Continuous tuning	2. Complex bias circuitry
Optical switch	1. No biasing line	1. Bulky
	2. Less interference	2. Complicated to integration
Physical switch	1. No bias line	1. Response time slow
	2. Continuous tuning	2. Complicated to integration

4.3. Fabrication Process of 5G mm-Wave Antennas

After simulating and optimizing the design in software, there are several methods to fabricate the antennas. The fabrication accuracy is an essential factor in fabricating an antenna at mm-Wave frequency band. The fabrication error in design dimension is responsible for shifting the resonant frequency. In photolithography fabrication process, various chemicals are used to mill out a selected area. Chemical etching is a wide popular method to produce high resolution complex patterns [114]. The limitations of this technology are its complex process, requirement of clean room, uses of hazardous chemicals, and large number of waste leftovers. Inkjet printing is another popular process for RF circuits and antenna fabrication. The high conductive ink using silver nano-structural material is widely used to produce compact designs with tiny details [115]. Three basic steps of inkjet printing process are printing, sintering, and characterization. Printing process depends on the composition of ink viscosity, conductivity, surface tension, and particle size. The automatic inkjet printer with user's controlled computer is used for printing process. The ink droplets are controlled from the nozzle to the specified position, so wastage of material is controlled [116]. The sintering process is helpful to increase the conductivity of the printing layer. The characterization involves the analysis of crack, surface roughness, etc. in the case of bending conformal structures. Screen printing is a cost effective and simple technique based on woven screen and different densities. To fabricate a design pattern, a squeegee blade and screen with ink are used [117]. This fabrication technology is useful for polyester and stainless steel.

The laser-milling machines are commonly used for rigid and flexible substrates for mm-Wave antennas. It provides precise fabrication with high accuracy for commercially available copper cladding and different variations in the thickness of substrate [118]. Printed circuit board (PCB) milling machines are highly efficient for electronic circuits and antenna fabrication. It is an automated system with milling/routing/drilling bits to etch the copper in a require manner from the surface of copper cladded PCB board. This technology became popular and well suited for mass production due to low cost and accurate antenna fabrication on a flexible substrate [119–120].

4.4. Specific Measurement Techniques of mm-Wave Antennas

Antenna measurement plays an important role in the antenna design cycle. The parameters of antenna-under-test (AUT) such as directivity, gain, reflection co-efficient, polarization, impedance, and efficiency are measured in the far-field region of an antenna. In measurement setup, the AUT can be used as either transmitting or receiving antenna, but for making easy measurement of the AUT, it is mostly used as a receiving antenna. For mm-Wave applications, the size of antenna element becomes very small and creates minor reflections as compared to microwave antennas. The challenges in the measurement of antenna need to address judiciously. Firstly, there are larger losses due to transmission line such as coaxial cable and waveguide. Secondly, the size of cable, connector, and probe used with AUT is larger

than antenna size. Thirdly, the fabrication demand of mm-Wave antenna is increasing due to using LTCC [121]. The various measurement setups for mm-Wave antennas are as follows.

4.4.1. Measurement Setup for Ka-Band

The measurement setup used for Ka-band is designed with a probe station, a GSG probe, a 2-port network analyzer, and a horn antenna as depicted in Fig. 24(a). A coplanar strip (CPS) balun structure fabricated on Si wafer is used to extract the antenna S-parameters. The distance between the horn antenna and AUT is about 40 cm. One port of network analyzer is connected to the horn antenna, and the other port is used to measure the differential S-parameters [122]. Gain is a standard parameter to analyze the antenna performance. Basically, gain is related to its direction of maximum radiation of antenna. The AUT is calibrated with a reference antenna in an anechoic chamber. The gain is measured in dBi by rotating the antenna in different directions, and a radiation pattern plot is created [123]. The radiation pattern measurement setup for Ka-band is shown in Fig. 24(b).

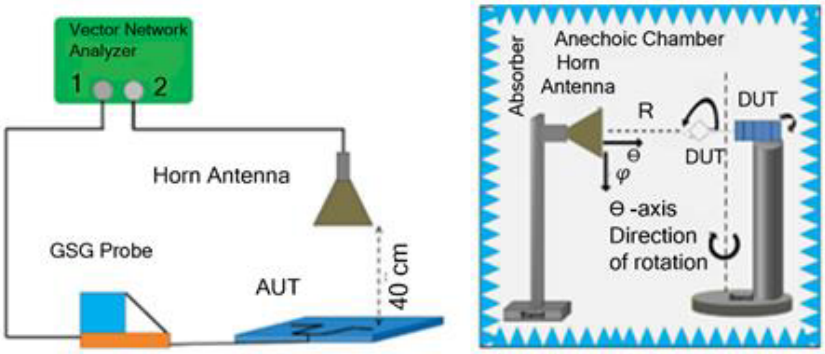

Figure 24. (a) Reflection coefficient measurement setup for Ka-band [122] and (b) radiation pattern measurement setup for Ka-band [123].

4.4.2. Measurement Setup for V-Band

The reflection coefficient measurement setup for V-band and 60 GHz is depicted in Figs. 25(a) and (b), respectively. A vector network analyser (VNA) with infinity I-67 ground signal ground (GSG) probe is used for reflection coefficient measurement. Line-reflect match method is used to calibrate the GSG probe with VNA [124, 125].

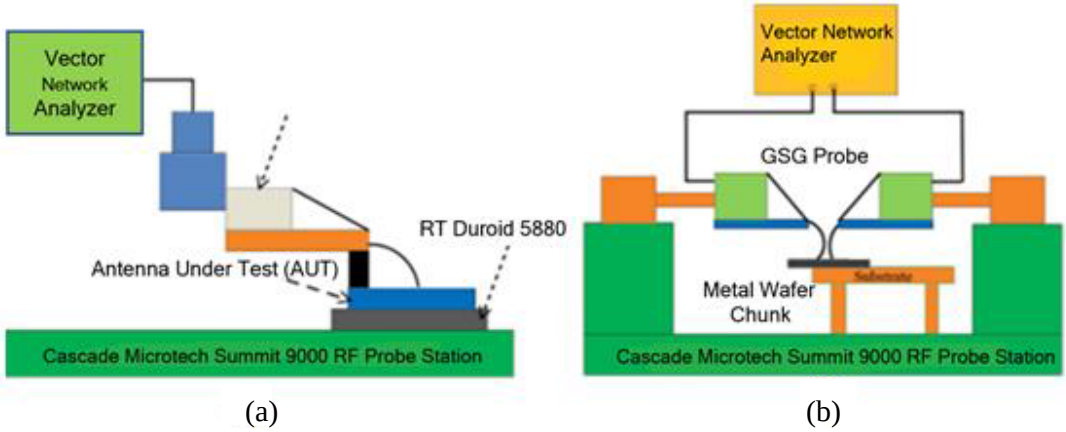

Figure 25. Reflection coefficient measurement setup (a) for V-band [124] and (b) for 60 GHz [125].

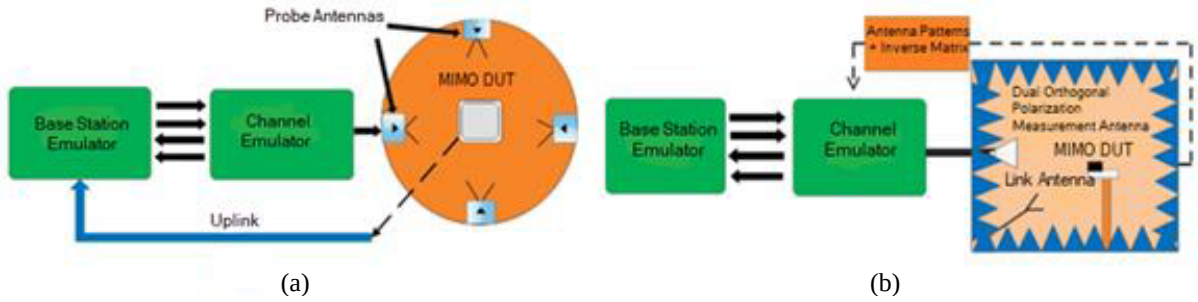

Figure 26. MIMO OTA setup (a) MPAC method [129] and (b) RTS method [130].

4.4.3. Measurement Setup for 5G-Massive MIMO Antennas

Massive MIMO is more mature for sub-6 GHz frequency band than mm-Wave. Over-the-air (OTA) tests are standardized methods for cellular telecommunication and internet association (CTIA) to measure the performance in wireless systems. OTA measurement system is useful for SISO antenna [126]. The measurement of MIMO antenna parameters is a critical and challenging task for 4G and upcoming 5G wireless technologies because they are very sensitive to noise, coupling, and correlation effect. The transmitted power levels in MIMO technology are different for different types of devices which change the device physical temperature. This temperature increases the noise temperature and is responsible for changing the throughput of the device under test (DUT) [127]. Two standard methods used in literature for MIMO antenna parameters measurement are multi-probe anechoic chamber (MPAC) and radiated two-stage (RTS) methods as shown in Fig. 26.

Figure 26(a) shows the standard MPAC measurement method for 4G MIMO OTA and 5G MIMO antennas. For measurement in MPAC method, the DUT is placed in the centre of an anechoic chamber with minimum eight dual-polarized probe antennas within a ring to imitate the model. The signal is delivered to probe antennas to create propagation with DUT by rotating for different angles after simulation of the signal by channel emulator. The MPAC method is not practical to perform 3-D MIMO test due to complexity and high cost [128]. Due to lower complexity and cheaper cost than MPAC method the RTS method is the favorable approach for future 5G MIMO antennas measurement as shown in Fig. 26(b). It has two measurement stages as in the first stage; the antenna pattern and inverse matrix of the propagation channels are measured. In the second stage, to generate the test signal, the pattern is loaded into the channel emulator. This test signal is then applied OTA to the receiving antennas and finally applied into the DUT to perform measurement [129, 130].

5. CONCLUSION

Due to attractive features of 5G technology, the researchers explored this technology for 5G applications. The concise study of this article makes it useful for academicians, researchers, and antenna designers to choose a suitable antenna to fulfill all the consumer requirements. The focus of this article is to investigate the design challenges and substrate selection at mm-Wave frequency band. The researchers have investigated various techniques to achieve high gain, high isolation, and circular polarization behavior. It is found that signal fading due to poor weather condition is resolved by using AMC reflector surfaces, antenna array, SIW antenna array, and multilayer structures techniques to achieve high gain. The MIMO antennas and massive MIMO antennas at base station are the possible solutions of NLOS propagation. The multipath propagation problem can be minimized by designing circularly polarized antennas. The measurement setup is set to compensate these challenges with reflection coefficient, gain, and radiation pattern measurement. This article explains the research trends and developments made in the fabrication and measurement of 5G mm-Wave antennas. In a nutshell, this article is expected to provide an excellent platform to inspire the researchers to bring forward valuable solutions for 5G technology. In future, more studies need to explore the research in revolutionary field of smart phones, 5G IoT, base stations, and mobile terminals. The 5G antennas will play a vital role in 5G technology, and by the inclusion of 5G technology with artificial intelligence (AI) system, a smart environment can be developed to realize smart things.

REFERENCES

1. Rappaport, T. S., *Wireless Communications: Principles and Practice*, 2nd Edition, Prentice Hall PTR, New Jersey, 1996.
2. Goldsmith, A., *Wireless Communications*, Cambridge University Press, 2005.
3. Hillebrand, F., "The creation of standards for global mobile communication: GSM and UMTS standardization from 1982 to 2000," *IEEE Wirel. Commun.*, Vol. 20, No. 4, 24–33, 2013.
4. Saeed, N., A. Bader, T. Y. Al-Naffouri, and M. S. Alouini, "When wireless communication faces COVID-19: Combating the pandemic and saving the economy," *Frontiers in Communications and Networks*, Vol. 1, No. 2, 2020.
5. Bliss, D. W. and S. Govindasamy, *Adaptive Wireless Communications: MIMO Channels and Networks*, Cambridge University Press, 2013.
6. Dahlman, E., S. Parkvall, and J. Skold, *4G: LTE/LTE-advanced for Mobile Broadband*, Academic Press, 2013.
7. Biglieri, E., R. Calderbank, A. Constantinides, A. Goldsmith, A. Paulraj, and H. V. Poor, *MIMO Wireless Communications*, Cambridge University Press, 2007.
8. Hampton, J. R., *Introduction to MIMO Communications*, Cambridge University Press, 2013.
9. Moradikordalivand, A., C. Y. Leow, T. AbdRahman, S. Ebrahimi, and T. H. Chua, "Wideband MIMO antenna system with dual polarization for Wi-Fi and LTE applications," *Int. J. Microw. Wireless Technol.*, Vol. 8, No. 2, 643–650, 2020.
10. Warren, D. and D. Calum, "Understanding 5G: Perspectives on future technological advancements in mobile," *GSMA Intelligence Report*, 2014.
11. https://www.ericsson.com/en/press-releases/2018/11/5g-estimated-to-reach-1.5-billion-subscriptions-in-2024-ericsson-mobility-report, 2018.
12. Matin, M. A., "Review on millimeter wave antennas-potential candidate for 5G enabled applications," *Advanced Electromagnetics*, Vol. 5, No. 2, 98–105, 2016.
13. Chih-Lin, I., S. Han, Z. Xu, Q. Sun, and Z. Pan, "5G: Rethink mobile communications for 2020," *Philosophical Trans. Royal Society A: Mathematical, Physical and Engineering Sciences*, Vol. 374, No. 2062, 20140432, 2016.
14. https://www.qualcomm.com/media/documents/files/5g-vision-use-cases.pdf.
15. Gawas, A. U., "An overview on evolution of mobile wireless communication networks: 1G–6G," *Int. J. Recent and Innovation Trends in Computing and Communication*, Vol. 3, No. 4, 3130–3133, 2015.
16. Anguera, J., A. Andújar, M. C. Huynh, C. Orlenius, C. Picher, and C. Puente, "Advances in antenna technology for wireless handheld devices," *Int. J. Antennas Propag.*, 1–25, 2013.
17. Lam, K. Y., K. M. Luk, K. F. Lee, H. Wong, and K. B. Ng, "Small circularly polarized U-slot wideband patch antenna," *IEEE Antennas Wirel. Propag. Lett.*, Vol. 10, 87–90, 2011.
18. Sharawi, M. S., "Printed multi-band MIMO antenna systems and their performance metrics [wireless corner]," *IEEE Antennas Propag. Mag.*, Vol. 55, No. 4, 218–232, 2013.
19. Li, Y., J. Wang, and K. M. Luk, "Millimeter-wave multibeam aperture-coupled magnetoelectric dipole array with planar substrate integrated beamforming network for 5G applications," *IEEE Trans. Antennas Propag.*, Vol. 65, No. 12, 6422–6431, 2017.
20. Yu, B., K. Yang, and G. Yang, "A novel 28 GHz beam steering array for 5G mobile device with metallic casing application," *IEEE Trans. Antennas Propag.*, Vol. 66, No. 1, 462–466, 2017.
21. Boxall, A., www.digitaltrends.com/mobile/xiaomi-mi-mix-3-news, 2019.
22. Boxall, A., www.digitaltrends.com/android/samsung-galaxy-s10-5g-news, 2019.
23. Simruni, M. and S. Jam, "Radiation performance improvement of wideband microstrip antenna array using wideband AMC structure," *Int. J. Communication Systems*, Vol. 32, No. 11, e3962, 2019.

24. Das, S., T. Bose, and H. Islam, "Design, and acceptance test of compact planar monopole antenna for LTE smartphone considering SAR, TRP, and HAC values," *Int. J. Communication Systems*, Vol. 32, No. 18, e4155, 2019.
25. Kraus, J. D., R. J. Marhefka, and A. S. Khan, *Antennas and Wave Propagation*, Tata McGraw-Hill Education, 2006.
26. Balanis, C. A., *Antenna Theory: Analysis and Design*, John Wiley & Sons, 2015.
27. Yu, G., G. Y. Li, L. C. Wang, A. Maaref, J. Lee, and D. Lopez-Perez, "Guest editorial: LTE in unlicensed spectrum," *IEEE Wirel. Commun.*, Vol. 23, No. 5, 6–7, 2016.
28. https://gsacom.com/5G-spectrum-bands, 2017.
29. https://www.fcc.gov/document/fcc-adopts-rules-facilitate-next-generation-wireless-technologies, 2016.
30. https://rspg-spectrum.eu/wp-content/uploads/2013/05/RPSG16-032-Opinion_5G.pdf, 2016.
31. Marcus, M. J., "5G and IMT for 2020 and beyond. [Spectrum Policy and Regulatory Issues]," *IEEE Wirel. Commun.*, Vol. 22, No. 3, 2–3, 2015.
32. https://www.qualcomm.com/news/onq/2017/10/04/path-opening-more-spectrum-5g-us, 2017.
33. Joint Task Group. ITUR, Annex 3 to Joint Task Group 4-5-6-7 Chairman's Report — Working document towards preliminary draft CPM text for WRC-15 agenda item 1.1. Tech. Rep. Doc. 2013; 4-5-6-7/393-E.
34. Resolution ITUR. 233. Studies on frequency-related matters on international mobile telecommunications and other terrestrial mobile broadband applications. Tech. Rep. 2012; 233 [COM6/8].
35. https://www.miwv.com/5g-radio-frequency, 2018.
36. MacCartney, G. R., J. Zhang, S. Nie, and T. S. Rappaport, "Path loss models for 5G millimeter wave propagation channels in urban microcells," *2013 IEEE Global Communications Conference (GLOBECOM)*, 3948–3953, 2013.
37. https://www.cablefree.net/wirelesstechnology/4glte/5g-frequency-bands-lte/.
38. Andrews, J. G., S. Buzzi, W. Choi, S. V. Hanly, A. Lozano, A. C. Soong, and J. C. Zhang, "What will 5G be?," *IEEE J. Selected Areas Communications*, Vol. 32, No. 5, 1065–1082, 2014.
39. Niu, Y., Y. Li, D. Jin, L. Su, and A. V. Vasilakos, "A survey of millimeter wave communications (mmWave) for 5G: Opportunities and challenges," *Wireless Networks*, Vol. 21, No. 8, 2657–2676, 2015.
40. Rappaport, T. S., J. N. Murdock, and F. Gutierrez, "State of the art in 60-GHz integrated circuits and systems for wireless communications," *Proc. of the IEEE*, Vol. 99, No. 8, 1390–1436, 2011.
41. Jameel, F., Z. Hamid, F. Jabeen, S. Zeadally, and M. A. Javed, "A survey of device-to-device communications: Research issues and challenges," *IEEE Commun. Surveys & Tutorials*, Vol. 20, No. 2, 2133–2168, 2018.
42. Chiaraviglio, L., C. Di Paolo, and N. B. Melazzi, "5G network planning under service and EMF constraints: Formulation and solutions," *IEEE Trans. Mobile Computing*, 1–18, 2021.
43. Jaber, M., M. A. Imran, R. Tafazolli, and A. Tukmanov, "5G backhaul challenges and emerging research directions: A survey," *IEEE Access*, Vol. 4, 1743–1766, 2016.
44. Ahmad, I., T. Kumar, M. Liyanage, J. Okwuibe, M. Ylianttila, and A. Gurtov, "Overview of 5G security challenges and solutions," *IEEE Commun. Standards Mag.*, Vol. 2, No. 1, 36–43, 2018.
45. https://www.bench.com/setting-the-benchmark/challenges-when-selecting-the-right-substrate-board-material-to-make-a-5g-mmwave-antenna, 2019.
46. https://rogerscorp.com/-/media/project/rogerscorp/documents/advanced-connectivity-solutions/english/data-sheets/rt-duroid-5870–5880-data-sheet.pdf.
47. https://rogerscorp.com/-/media/project/rogerscorp/documents/advanced-connectivity-solutions/english/data-sheets/ro3000-laminate-data-sheet-ro3003–ro3006–ro3010–ro3035.pdf.
48. https://rogerscorp.com/-/media/project/rogerscorp/documents/advanced-connectivity-solutions/english/data-sheets/ro4000-laminates-ro4003c-and-ro4350b-data-sheet.pdf.

49. https://en.wikipedia.org/wiki/FR-4.
50. Zhang, L., S. Zhao, P. Shang, J. Liu, and F. Han, "Distributed adaptive range extension setting for small cells in heterogeneous cellular network," *2017 IEEE 85th Vehicular Technology Conference (VTC Spring)*, 1–7, 2017.
51. Mehran, F. and A. Rahimian, "Physical layer performance enhancement for femtocell SISO/MISO soft real-time wireless communication systems employing serial concatenation of quadratic interleaved codes," *IEEE 20th Iranian Conference on Electrical Engineering (ICEE2012)*, 1188–1193, 2012.
52. Bouras, C. and G. Diles, "Energy efficiency in sleep mode for 5G femtocells," *2017 IEEE Wireless Days*, 143–145, 2017.
53. Wang, C.-J. and C.-H. Lin, "A circularly polarized quasi-loop antenna," *Progress In Electromagnetics Research*, Vol. 84, 333–348, 2008.
54. Khalily, M., R. Tafazolli, T. A. Rahman, and M. R. Kamarudin, "Design of phased arrays of series-fed patch antennas with reduced number of the controllers for 28-GHz mm-wave applications," *IEEE Antennas Wirel. Propag. Lett.*, Vol. 15, 1305–1308, 2015.
55. Ta, S. X., H. Choo, and I. Park, "Broadband printed-dipole antenna, and its arrays for 5G applications," *IEEE Antennas Wirel. Propag. Lett.*, Vol. 16, 2183–2186, 2017.
56. Dadgarpour, A., M. S. Sorkherizi, and A. A. Kishk, "Wideband low loss magnetoelectric dipole antenna for 5G wireless network with gain enhancement using meta lens and gap waveguide technology feeding," *IEEE Trans. Antennas Propag.*, Vol. 64, No. 12, 5094–5101, 2016.
57. Park, S. J., D. H. Shin, and S. O. Park, "Low side-lobe substrate-integrated-waveguide antenna array using broadband unequal feeding network for millimeter-wave handset device," *IEEE Trans. Antennas Propag.*, Vol. 64, No. 2, 923–932, 2015.
58. Ali, M., K. K. Sharma, R. P. Yadav, A. Kumar, F. Jiang, Q. S. Cheng, and G. L. Huang, "Design of dual mode wideband SIW slot antenna for 5G applications," *Int. J. RF Microw. Comput.-Aided Engineering*, Vol. 30, No. 12, e22449, 2020.
59. Ullah, H. and F. A. Tahir, "A wide-band rhombus monopole antenna array for millimeter wave applications," *Microw. Optical Technol. Lett.*, Vol. 62, No. 4, 2111–2117, 2020.
60. Yang, W. C., H. Wang, W. Q. Che, Y. Huang, and J. Wang, "High-gain, and low-loss millimeter-wave LTCC antenna array using artificial magnetic conductor structure," *IEEE Trans. Antennas Propag.*, Vol. 63, No. 1, 390–395, 2014.
61. Cheng, Y. and Y. Dong, "A compact folded SIW multibeam antenna array for 5G millimeter wave applications," *Microw. Optical Technol. Lett.*, Vol. 63, No. 3, 1236–1242, 2021.
62. Malathi, A. C. J. and D. Thiripurasundari, "Review on isolation techniques in MIMO antenna systems," *Indian Journal of Science and Technology*, Vol. 9, No. 35, 1–10, 2016.
63. Sharawi, M. S., "Printed multi-band MIMO antenna systems and their performance metrics [wireless corner]," *IEEE Antennas Propag. Mag.*, Vol. 55, No. 4, 218–232, 2013.
64. Blanch, S., J. Romeu, and I. Corbella, "Exact representation of antenna system diversity performance from input parameter description," *Electron. Lett.*, Vol. 39, No. 9, 705–707, 2003.
65. Hallbjorner, P., "The significance of radiation efficiencies when using S-parameters to calculate the received signal correlation from two antennas," *IEEE Antennas Wirel. Propag. Lett.*, Vol. 4, 97–99, 2005.
66. Rosengren, K. and P. S. Kildal, "Radiation efficiency, correlation, diversity gain and capacity of a six-monopole antenna array for a MIMO system: Theory, simulation, and measurement in reverberation chamber," *IEE Proceedings — Microwaves, Antennas and Propagation*, Vol. 152, No. 1, 7–16, 2005.
67. Chae, S. H., S. K. Oh, and S. O. Park, "Analysis of mutual coupling, correlations, and TARC in WiBro MIMO array antenna," *IEEE Antennas Wirel. Propag. Lett.*, Vol. 6, 122–125, 2007.
68. Shin, H. and J. H. Lee, "Capacity of multiple antennas fading channels: Spatial fading correlation, double scattering, and keyhole," *IEEE Trans. Information Theory*, Vol. 49, No. 10, 2636–2647, 2003.

69. Jilani, S. F. and A. Alomainy, "Millimeter-wave T-shaped MIMO antenna with defected ground structures for 5G cellular networks," *IET Microw., Antennas & Propag.*, Vol. 12, No. 4, 672–677, 2018.
70. Lin, M., P. Liu, and Z. Guo, "Gain-enhanced Ka-band MIMO antennas based on the SIW corrugated technique," *IEEE Antennas Wirel. Propag. Lett.*, Vol. 16, 3084–3087, 2017.
71. Khalid, M., S. IffatNaqvi, N. Hussain, M. Rahman, S. S. Mirjavadi, M. J. Khan, and Y. Amin, "4-port MIMO antenna with defected ground structure for 5G millimeter wave applications," *Electronics*, Vol. 9, No. 1, 71, 2020.
72. Zhang, Y., J. Y. Deng, M. J. Li, D. Sun, and L. X. Guo, "A MIMO dielectric resonator antenna with improved isolation for 5G mm-wave applications," *IEEE Antennas Wirel. Propag. Lett.*, Vol. 18, No. 3, 747–751, 2019.
73. Sharma, S., B. K. Kanaujia, and M. K. Khandelwal, "Implementation of four-port MIMO diversity microstrip antenna with suppressed mutual coupling and cross-polarized radiations," *Microsystem Technologies*, Vol. 26, No. 2, 993–1000, 2020.
74. Ikram, M., M. S. Sharawi, K. Klionovski, and A. Shamim, "A switched-beam millimeter-wave array with MIMO configuration for 5G applications," *Microw. Optical Technol. Lett.*, Vol. 60, No. 3, 915–920, 2018.
75. Wani, Z., M. P. Abegaonkar, and S. K. Koul, "A 28-GHz antenna for 5G MIMO applications," *Progress In Electromagnetics Research Letters*, Vol. 78, 73–79, 2018.
76. Gupta, S., Z. Briqech, A. R. Sebak, and T. A. Denidni, "Mutual-coupling reduction using metasurface corrugations for 28 GHz MIMO applications," *IEEE Antennas Wirel. Propag. Lett.*, Vol. 16, 2763–2766, 2017.
77. Usman, M., E. Kobal, J. Nasir, Y. Zhu, C. Yu, and A. Zhu, "Compact SIW fed dual-port single element annular slot MIMO antenna for 5G mmWave applications," *IEEE Access*, Vol. 9, 91995–92002, 2021.
78. Kumar, A., A. Q. Ansari, B. K. Kanaujia, J. Kishor, and L. Matekovits, "A review on different techniques of mutual coupling reduction between elements of any MIMO antenna. Part 1: DGSs and parasitic structures," *Radio Science*, Vol. 56, No. 2, e2020RS007122, 2021.
79. Nadeem, I. and D.-Y. Choi, "Study on mutual coupling reduction techniques for MIMO antennas," *IEEE Access*, Vol. 7, 563–586, 2018.
80. Han, T. Y., "Broadband circularly polarized square-slot antenna," *Journal of Electromagnetic Waves and Applications*, Vol. 22, No. 3, 549–554, 2008.
81. Hussain, N., M. J. Jeong, J. Park, and N. Kim, "A broadband circularly polarized fabry-perot resonant antenna using a single-layered PRS for 5G MIMO applications," *IEEE Access*, Vol. 7, 42897–42907, 2019.
82. Chen, H., Y. Shao, Y. Zhang, C. Zhang, and Z. Zhang, "A low-profile broadband circularly polarized mmWave antenna with special-shaped ring slot," *IEEE Antennas Wirel. Propag. Lett.*, Vol. 18, No. 6, 1492–1496, 2019.
83. Kumar, A., A. Kumar, and A. Kumar, "A broadband circularly polarized monopole antenna for millimeter-wave short range 5G wireless communication," *Int. J. RF Microw. Comput.-Aided Engineering*, Vol. 31, No. 1, e22518, 2021.
84. Jian, R., Y. Chen, and T. Chen, "Compact wideband circularly polarized antenna with symmetric parasitic rectangular patches for Ka-band applications," *Int. J. Antennas Propag.*, 1–8, 2019.
85. Wu, Q., J. Hirokawa, J. Yin, C. Yu, H. Wang, and W. Hong, "Millimeter-wave multibeam end fire dual-circularly polarized antenna array for 5G wireless applications," *IEEE Trans. Antennas Propag.*, Vol. 66, No. 9, 4930–4935, 2018.
86. Park, S. J. and S. O. Park, "LHCP and RHCP substrate integrated waveguide antenna arrays for millimeter-wave applications," *IEEE Antennas Wirel. Propag. Lett.*, Vol. 16, 601–604, 2016.
87. Du, M., J. Xu, X. Ding, J. Cao, J. Deng, and Y. Dong, "A low-profile wideband LTCC integrated circularly polarized helical antenna array for millimeter-wave applications," *Radioengineering*, Vol. 27, No. 1, 455–462, 2018.

88. Lin, W. and R. W. Ziolkowski, "Compact, omni-directional, circularly polarized mm-Wave antenna for device-to-device (D2D) communications in future 5G cellular systems," *2017 10th Global Symposium on Millimeter-Waves*, 115–116, 2017.
89. Qing, X. and Z. N. Chen, "Millimeter-wave broadband circularly polarized stacked microstrip antenna for satellite applications," *2016 IEEE 5th Asia-Pacific Conference on Antennas and Propagation (APCAP)*, 341–342, 2016.
90. Mantash, M. and T. A. Denidni, "3D FSS polarizer for millimeter-wave antenna applications," *Int. J. RF Microw. Comput.-Aided Engineering*, Vol. 29, No. 8, e21767, 2019.
91. Hesari, S. S. and J. Bornemann, "Wideband circularly polarized substrate integrated waveguide end fire antenna system with high gain," *IEEE Antennas Wirel. Propag. Lett.*, Vol. 16, 2262–2265, 2017.
92. Yoon, S. J. and J. H. Choi, "A Ka-band circular polarized waveguide slot antenna with a cross iris," *Applied Sciences*, Vol. 10, No. 19, e6994, 2020.
93. Zhang, K., J. Li, Y. Yang, and R. Xu, "A novel design of circularly polarized waveguide antenna," *Proceedings of 2014 3rd IEEE Asia-Pacific Conference on Antennas and Propagation*, 130–133, 2014.
94. Kesavan, A., M. A. Al-Hassan, I. Ben Mabrouk, and T. A. Denidni, "Wideband circular polarized dielectric resonator antenna array for millimeter-wave applications," *Sensors*, Vol. 21, No. 11, e3614, 2021.
95. Askari, H., N. Hussain, M. A. Sufian, S. M. Lee, and N. Kim, "A wideband circularly polarized magnetoelectric dipole antenna for 5G millimeter-wave communications," *Sensors*, Vol. 22, 2338, 2022.
96. Zhu, C., G. Xu, D. Ding, J. Wu, W. Wang, Z.-X. Hunag, and X.-L. Wu, "Low-profile wideband millimeter-wave circularly polarized antenna with hexagonal parasitic patches," *IEEE Antennas Wirel. Propag. Lett.*, Vol. 20, No. 9, 1651–1655, 2021.
97. Khalid, M., S. IffatNaqvi, N. Hussain, M. Rahman, S. S. Mirjavadi, M. J. Khan, and Y. Amin, "4-port MIMO antenna with defected ground structure for 5G millimeter wave applications," *Electronics*, Vol. 9, No. 1, 71, 2020.
98. Christodoulou, C. G., Y. Tawk, S. A. Lane, and S. R. Erwin, "Reconfigurable antennas for wireless and space applications," *Proceedings of the IEEE*, Vol. 100, No. 6, 2250–2261, 2012.
99. Friis, H. T., C. B. Feldman, and W. M. Sharpless, "The determination of the direction of arrival of short radio waves," *Proceedings of the Institute of Radio Engineers*, Vol. 22, No. 1, 47–78, 1934.
100. Al Abbas, E., A. T. Mobashsher, and A. Abbosh, "Polarization reconfigurable antenna for 5G cellular networks operating at millimeter waves," *2017 IEEE Asia Pacific Microwave Conference (APMC)*, 772–774, 2017.
101. Brown, E. R., "RF-MEMS switches for reconfigurable integrated circuits," *IEEE Trans. Microw. Theory and Techniques*, Vol. 46, No. 11, 1868–1880, 1998.
102. Deng, Z., J. Gan, H. Wei, H. Gong, and X. Guo, "Ka-band radiation pattern reconfigurable antenna based on microstrip MEMS switches," *Progress In Electromagnetics Research Letters*, Vol. 59, 93–99, 2016.
103. Ikram, M., E. Al Abbas, N. Nguyen-Trong, K. H. Sayidmarie, and A. Abbosh, "Integrated frequency-reconfigurable slot antenna and connected slot antenna array for 4G and 5G mobile handsets," *IEEE Trans. Antennas Propag.*, Vol. 67, No. 12, 7225–7233, 2019.
104. Anagnostou, D. E., G. Zheng, M. T. Chryssomallis, J. C. Lyke, G. E. Ponchak, J. Papapolymerou, and C. G. Christodoulou, "Design, fabrication, and measurements of an RF-MEMS-based self-similar reconfigurable antenna," *IEEE Trans. Antennas Propag.*, Vol. 54, No. 1, 422–432, 2006.
105. Dufour, G., N. Tiercelin, W. T. Khan, P. Coquet, P. Pernod, and J. Papapolymerou, "Large frequency tuning of a millimeter-wave antenna using dielectric liquids in integrated micro-channels," *2015 IEEE MTT-S International Microwave Symposium*, 1–4, 2015.

106. Jilani, S. F., S. M. Abbas, K. P. Esselle, and A. Alomainy, "Millimeter-wave frequency reconfigurable T-shaped antenna for 5G networks," *2015 IEEE 11th International Conference on Wireless and Mobile Computing, Networking and Communications (WiMob)*, 100–102, 2015.
107. Hassan, A. E. H., N. Fadlallah, M. Rammal, G. Z. El Nashef, and E. Rachid, "Wideband reconfigurable millimeter-wave linear array antenna using liquid crystal for 5G networks," *Wireless Engineering and Technology*, Vol. 12, No. 1, 1–14, 2021.
108. Al Abbas, E., N. Nguyen-Trong, A. T. Mobashsher, and A. M. Abbosh, "Polarization-reconfigurable antenna array for millimeter-wave 5G," *IEEE Access*, Vol. 7, 131214–131220, 2019.
109. Haupt, R. L. and M. Lanagan, "Reconfigurable antennas," *IEEE Antennas Propag. Magazine*, Vol. 55, No. 1, 49–61, 2013.
110. Lai, M. I., T. Y. Wu, J. C. Hsieh, C. H. Wang, and S. K. Jeng, "Design of reconfigurable antennas based on an L-shaped slot and PIN diodes for compact wireless devices," *IET Microwaves, Antennas & Propagation*, Vol. 3, No. 1, 47–54, 2009.
111. Weedon, W. H., W. J. Payne, and G. M. Rebeiz, "MEMS-switched reconfigurable antennas," *IEEE Antennas and Propagation Society International Symposium. 2001 Digest. Held in conjunction with: USNC/URSI National Radio Science Meeting (Cat. No. 01CH37229)*, Vol. 3, 654–657, 2001.
112. Petosa, A., "An overview of tuning techniques for frequency-agile antennas," *IEEE Antennas Propag. Magazine*, Vol. 54, No. 4, 271–296, 2012.
113. Entesari, K. and A. P. Saghati, "Fluidics in microwave components," *IEEE Microwave Magazine*, Vol. 17, No. 5, 50–75, 2016.
114. Raymond, L., L. Nelson, D. Hamilton, and W. Kerwin, "Fabrication of passive components for high temperature instrumentation," *IEEE Trans. Components, Hybrids, and Manufacturing Technology*, Vol. 2, No. 3, 395–398, 1979.
115. Lakafosis, V., A. Rida, R. Vyas, L. Yang, S. Nikolaou, and M. M. Tentzeris, "Progress towards the first wireless sensor networks consisting of inkjet-printed, paper-based RFID-enabled sensor tags," *Proceedings of the IEEE*, Vol. 98, No. 9, 1601–1609, 2010.
116. Orecchini, G., F. Alimenti, V. Palazzari, A. Rida, M. M. Tentzeris, and L. Roselli, "Design and fabrication of ultra-low-cost radio frequency identification antennas and tags exploiting paper substrates and inkjet printing technology," *IET Microwaves, Antennas & Propagation*, Vol. 5, No. 8, 993–1001, 2011.
117. Gamota, D. R., P. Brazis, K. Kalyanasundaram, and J. Zhang, *Printed Organic and Molecular Electronics*, Springer Science & Business Media, 2013.
118. https://www.lpkf.com/en/industries-technologies/research-in-house-pcb-prototyping/produkte/-lpkf-protolaser-u4, 2017.
119. Jilani, S. F., A. Rahimian, Y. Alfadhl, and A. Alomainy, "Low-profile flexible frequency-reconfigurable millimeter-wave antenna for 5G applications," *Flexible and Printed Electronics*, Vol. 3, No. 2, 035003, 2018.
120. Tehrani, B., B. Cook, J. Cooper, and M. Tentzeris, "Inkjet printing of a wideband, high gain mm-wave Vivaldi antenna on a flexible organic substrate," *2014 IEEE Antennas and Propagation Society International Symposium (APSURSI)*, 320–321, 2014.
121. Balanis, C. A., *Antenna Theory: Analysis and Design*, John Wiley & Sons, 2015.
122. Shamim, A., L. Roy, N. Fong, and N. G. Tarr, "24 GHz on-chip antennas and balun on bulk Si for air transmission," *IEEE Trans. Antennas Propag.*, Vol. 56, No. 1, 303–311, 2008.
123. https://antennatestlab.com/antenna-education-tutorials/gain-dbi-passive-antenna.
124. Liu, C. C. and R. G. Rojas, "V-band integrated on-chip antenna implemented with a partially reflective surface in standard 0.13-µm BiCMOS technology," *IEEE Trans. Antennas Propag.*, Vol. 64, No. 12, 5102–5109, 2016.
125. Jing, L., C. R. Rowell, S. Raju, M. Chan, R. D. Murch, and C. P. Yue, "Fabrication and measurement of millimeter-wave on-chip MIMO antenna for CMOS RFIC's," *2016 IEEE MTT-S International Wireless Symposium (IWS)*, 1–4, 2016.

126. https://api.ctia.org/wpcontent/uploads/2019/04/CTIAOTATest_Plan_3_8_2.pdf, 2019.
127. Qi, Y., G. Yang, L. Liu, J. Fan, A. Orlandi, H. Kong, W. Yu, and Z. Yang, "5G over-the-air measurement challenges: Overview," *IEEE Trans. Electromagnetic Compatibility*, Vol. 59, No. 5, 1661–1670, 2017.
128. Li, J., Y. Qi, W. Yu, F. Li, J. Fan, A. Orlandi, Z. Yang, and S. Wu, "Objective MIMO measurement," *IEEE Trans. Electromagnetic Compatibility*, Vol. 60, No. 4, 1190–1197, 2018.
129. Yu, W., Y. Qi, K. Liu, Y. Xu, and J. Fan, "Radiated two-stage method for LTE MIMO user equipment performance evaluation," *IEEE Trans. Electromagnetic Compatibility*, Vol. 56, No. 5, 1691–1696, 2014.
130. Shen, P., Y. Qi, W. Yu, and F. Li, "Inverse matrix autosearch technique for the RTS MIMO OTA test," *IEEE Trans. Electromagnetic Compatibility*, Vol. 63, No. 3, 962–969, 2021.